Ultimate behaviour and serviceability analysis of stainless steel reinforced concrete beams

Musab Rabi[a, b], K.A. Cashell[a], Rabee Shamass[c]

[a] Dept of Civil Engineering, Jerash University, Jordan

[b] Dept of Civil and Environmental Engineering, Brunel University London, UK

[c] Division of Civil and Building Services Engineering, School of Build Environment and Architecture, London South Bank University, UK

Abstract

Stainless steel reinforcement has become a very attractive option for reinforced concrete structures owing to its distinctive properties including outstanding corrosion resistance, excellent fire behaviour, long life cycle as well as low maintenance requirements. Additionally, stainless steel reinforcement offers exceptional ductility and strain hardening characteristics compared with other common materials, which are very desirable in design to avoid sudden collapse. However, most global design standards do not incorporate an appropriate design approach for reinforced concrete members with stainless steel. The substantial strain hardening characteristics of stainless steel are typically not represented in standardised material models and therefore this attractive characteristic is not exploited in design resulting in structural and economic inefficiencies. Hence, the aim of this paper is to propose and validate a new deformation-based design approach for stainless steel reinforced concrete beams based on the continuous strength method, with reference to the current design rules provided in Eurocode 2. This approach is shown to be an effective design tool that exploits the distinctive characteristics of stainless steel reinforcement in an efficient and reliable manner. It is shown to provide a more efficient design with less over-conservatism and greater accuracy, compared with other methods. A comprehensive parametric study is conducted using Abaqus software to study the influence that various geometric and material properties have on the capacity of the members. Moreover, the serviceability limit state is also explored through a detailed analysis of the deflection behaviour.

Highlights

- The behaviour of stainless steel reinforced concrete beams is investigated.
- A full and simplified version of a deformation-based design method is proposed and examined herein with reference to the current design rules in Eurocode 2.
- A comprehensive parametric study is conducted to study the most influential parameters.
- The serviceability limit state is also explored through a detailed analysis of the deflection behaviour.

Keywords: Stainless steel; Reinforced concrete; Beams; Continuous strength method, Numerical analysis; Abaqus; Deflections; Eurocode 2.

1. Introduction

Stainless steel is an exceptional construction material that has recently become an attractive choice for reinforced concrete structures owing principally to its excellent corrosion resistance and durability. In addition, stainless steel exhibits favourable mechanical properties, great ductility, a long life cycle and is fully recyclable. These distinctive characteristics mainly depend on the constituent elements of the stainless steel alloys and thus it is essential to carefully select the appropriate grade for each particular application. Stainless steels are defined as a group of corrosion resistant, alloying steels which possess a minimum chromium content of 10.5% and a maximum carbon content of 1.2%. There are five main categories of stainless steel, and each grade is classified according to its metallurgical structure: (1) austenitic, (2) ferritic, (3) duplex, (4) martensitic and (5) precipitation hardened stainless steel [1].

The durability, resilience and efficiency of structures and infrastructure are highly topical at the current time, especially following the Polcevera Viaduct tragedy in Italy 2018 [2]. Whilst there are ever-increasing demands for civil engineering structures and infrastructure to be more durable, there are also significant pressures to achieve long service periods without requiring rehabilitative or remedial works, to be more efficient in terms of material usage, and to be more resilient to both natural and man-made environments and scenarios. It is estimated that Western Europe spends around €5 billion annually on

repairing corroding concrete infrastructure [3], with a corresponding figure of $8.3 billion for the United States [4]. In addition, there can be significant further indirect costs associated with important infrastructure being out-of-service. In this context, there is a clear motivation for improving the life of reinforced concrete (RC) elements, especially for those in sensitive or harsh environments such as bridges, tunnels and marine structures.

For structures subjected to aggressive conditions and reinforced with traditional carbon steel, corrosion is difficult to avoid. The typical approaches for improving durability are to control the alkalinity of concrete, increase the depth of concrete cover or use cement inhibitors or reinforcement coating materials. However, in harsh or exposed environments, all of these measures may not be sufficient to prevent the development of unacceptable levels of corrosion in which case, the use of stainless steel reinforcement may provide an ideal solution. Stainless steel reinforcement may even result in an increase in the life time of structures, and a significant reduction in the cost of expensive inspections and rehabilitation works.

There are a number of reasons that stainless steel reinforcement is not more commonly employed in every-day reinforced concrete structures. Firstly, there is a common perception amongst engineers that stainless steel reinforcement is prohibitively expensive, particularly in terms of their initial cost, and the full life cycle costs are not always considered when selecting the materials [5]. Secondly, there is a lack of design guidance and performance data available in the public domain, mainly owing to this being a relatively new topic in structural engineering terms. Given the high initial cost of stainless steel, it is crucial that efficient design rules which exploit the advantageous and distinctive properties of the material should be made available. However, most global design standards [6] do not incorporate an efficient design approach for RC members with stainless steel. In particular, they generally include an elastic-plastic material model for idealising the reinforcement behaviour, which does not exploit the significant strain hardening and high ductility characteristics of stainless steel. Although, this assumption could be acceptable for the design of traditional concrete structures reinforced with carbon steel, it results in inaccurate predictions for stainless steel RC members since stainless steel exhibits a

78 nonlinear response from an early stage followed by significant strain hardening. Therefore, designing
79 RC structures with stainless steel using the current design rules, is neither efficient nor accurate.

80 There has been extensive research in recent years into the behaviour of structural stainless steel
81 including retrofitting applications [7, 8], the flexural behaviour [9, 10], compressive response [11, 12]
82 and the mechanical characteristics [13-15]. However, most of this research has focused on bare stainless
83 steel sections, rather than stainless steel reinforced concrete which is the main concern of the current
84 paper. There has been some research in recent years into the flexural behaviour of reinforced concrete
85 beams which were repaired using a hybrid system of stainless steel rebars and CFRP sheets [16].
86 Recently, Hasan et al. has investigated a series of geographical locations which are suitable for using
87 stainless steel rebars in reinforced concrete girder bridges using a life cycle costing (LCC) based system
88 [17]. However, the current paper is concerned with the behaviour of stainless steel reinforced concrete
89 flexural members, and the principal objective is to propose and validate an alternative design method
90 to those available in the current design standards. The proposed method is based on the increasingly
91 popular continuous strength method (CSM), which is a deformation-based design approach that
92 harnesses the advantages of material strain hardening. The CSM was originally developed for stainless
93 steel structural members with non-slender cross-sections [18] and has been developed many times over
94 the last 15 years [19-21]. The approach has also been adapted for composite construction [22; 23] and
95 has most recently been extended to include RC beams reinforced with stainless steel [24]. This paper
96 presents the results of a comprehensive parametric study in which the most influential geometric and
97 material properties are examined, in terms of the structural performance of stainless steel RC members.
98 Building on previous work, the CSM approach is examined over an extensive range of parameters, with
99 emphasis given to the geometry of the section, reinforcement ratio and also deflections, in the context
100 of the nonlinear stress-strain behaviour.

101 ## 2. Design of stainless steel reinforced concrete beams

102 Two versions of the continuous strength method (CSM) have been developed for the design of stainless
103 steel reinforced concrete beams, accounting for the distinct material properties of the reinforcement.

The full analytical model (hereafter referred to as AM) considers the full stress-strain response of stainless steel whereas the simplified model (SM) considers simplified material model for the stainless steel which is a bilinear elastic-linear strain hardening relationship; these are both presented in Fig. 1. The full details of these models are available in [24], and a concise overview is presented herein.

2.1. Material model

The constitutive behaviour of stainless steel is noticeably different from that of carbon steel, as shown in Fig. 2. Stainless steel exhibits a nonlinear response from the beginning, does not have a clearly defined yield point and develops significant strain hardening and ductility. In contrast, carbon steel exhibits a linear relationship in the elastic range with a well-defined yield point, followed by a moderate degree of stain hardening. Hence, the 0.2% proof stress ($\sigma_{0.2}$) is typically used to identify the yield limit in stainless steel.

The modified Ramberg-Osgood stainless steel material model developed by Mirambell and Real [14] and Rasmussen [15], which is an extension of the original version [13], is employed to represent the stainless steel constitutive stress-strain relationship. This material model was developed on the basis of empirical data and has been adopted in an extensive number of research papers [18-25]. It includes the two expressions presented in Eqs. 1 and 2, for the elastic and non-elastic stages of the behaviour, respectively:

$$\varepsilon = \frac{\sigma}{E} + 0.002\left(\frac{\sigma}{\sigma_{0.2}}\right)^{n} \quad \text{for} \quad \sigma \leq \sigma_{0.2} \tag{1}$$

$$\varepsilon = \varepsilon_{0.2} + \frac{\sigma-\sigma_{0.2}}{E_2} + \left(\varepsilon_u - \varepsilon_{0.2} - \frac{\sigma_u-\sigma_{0.2}}{E_2}\right)\left(\frac{\sigma-\sigma_{0.2}}{\sigma_u-\sigma_{0.2}}\right)^{m} \quad \text{for} \quad \sigma_{0.2} < \sigma \leq \sigma_u \tag{2}$$

In these expressions, ε and σ are the engineering strain and stress, respectively; E is the elastic modulus; E_2 is the tangent modulus at the 0.2% proof stress; σ_u and ε_u are the ultimate stress and corresponding strain, respectively; $\varepsilon_{0.2}$ is the strain corresponding to $\sigma_{0.2}$; and n and m are material constants related to the strain hardening behaviour. It is noteworthy that all equations in this paper are applied using SI units, unless stated otherwise.

126 However, in order to implement the material model in conjunction with the design method, it is
127 necessary to determine the stress as a function of strain. Therefore, the inversion relationship proposed
128 by [26] for the full stress-strain relationship of stainless steel is employed, as presented in Eqs. 3 and 4.

$$\sigma_1(\varepsilon) = \sigma_{0.2}\frac{r\left(\frac{\varepsilon}{\varepsilon_{0.2}}\right)}{1+(r-1)\left(\frac{\varepsilon}{\varepsilon_{0.2}}\right)^p} \qquad \text{for} \quad \varepsilon \le \varepsilon_{0.2} \tag{3}$$

129

$$\sigma_2(\varepsilon) = \sigma_{0.2}\left[1+\frac{r_2\left[\frac{\varepsilon}{\varepsilon_{0.2}}-1\right]}{1+(r^*-1)\left(\frac{\frac{\varepsilon}{\varepsilon_{0.2}}-1}{\frac{\varepsilon_u}{\varepsilon_{0.2}}-1}\right)^{p^*}}\right] \qquad \text{for} \quad \varepsilon > \varepsilon_{0.2} \tag{4}$$

130 where the material parameters are:

$$\varepsilon_{0.2} = \frac{\sigma_{0.2}}{E} + 0.002 \qquad r = \frac{E\,\varepsilon_{0.2}}{\sigma_{0.2}}$$

$$E_2 = \frac{E}{1+0.002\,n/e} \qquad p = r\frac{1-r_2}{r-1}$$

$$e = \frac{\sigma_{0.2}}{E} \qquad m = 1+3.5\frac{\sigma_{0.2}}{\sigma_u}$$

$$\sigma_u = \sigma_{0.2}\frac{1-0.0375(n-5)}{0.2+185e} \qquad E_u = \frac{E_2}{1+(r^*-1)m}$$

$$r_2 = \frac{E_2\,\varepsilon_{0.2}}{\sigma_{0.2}} \qquad r_u = \frac{E_u(\varepsilon_u-\varepsilon_{0.2})}{\sigma_u-\sigma_{0.2}}$$

$$\varepsilon_u = \min\left(1-\frac{\sigma_{0.2}}{\sigma_u}, A\right) \qquad p^* = r^*\frac{1-r_u}{r^*-1}$$

$$r^* = \frac{E_2(\varepsilon_u-\varepsilon_{0.2})}{\sigma_u-\sigma_{0.2}} \qquad n = \frac{\ln(20)}{\ln(\sigma_{0.2}/\sigma_{0.01})}$$

131 In these expressions, A is the stainless steel elongation; E_u is the slope of the stress-strain curve at ε_u;
132 and r, r_2, r*, r_u, p and p* are parameters that need to be determined.

For the simplified design model, a bilinear stress-strain relationship is employed to avoid the complexity of nonlinear equations, as presented in Eqs. 5 and 6, and depicted in Fig. 1. In this approach, the yield point is identified as the 0.2% proof stress ($\sigma_{0.2}$) and the corresponding yield strain (ε_y) is determined by dividing this value by the elastic modulus, E. The difference between ε_y and $\varepsilon_{0.2}$ as employed in the full analytical model are demonstrated in Fig. 1. The slope of the strain hardening region (E_{sh}) is obtained from the line passing through the yield (ε_y, $\sigma_{0.2}$) and ultimate ($C_2\varepsilon_u$, σ_u) points, as defined in Eq. 7. It has been found that a value of 0.15 is an appropriate value for the constant C_2 [24].

$$\sigma = E\varepsilon \qquad \varepsilon \leq \varepsilon_y \tag{5}$$

$$\sigma = \sigma_{0.2} + E_{sh}(\varepsilon - \varepsilon_y) \qquad \varepsilon > \varepsilon_y \tag{6}$$

$$E_{sh} = \frac{\sigma_u - \sigma_{0.2}}{C_2\varepsilon_u - \varepsilon_y} \tag{7}$$

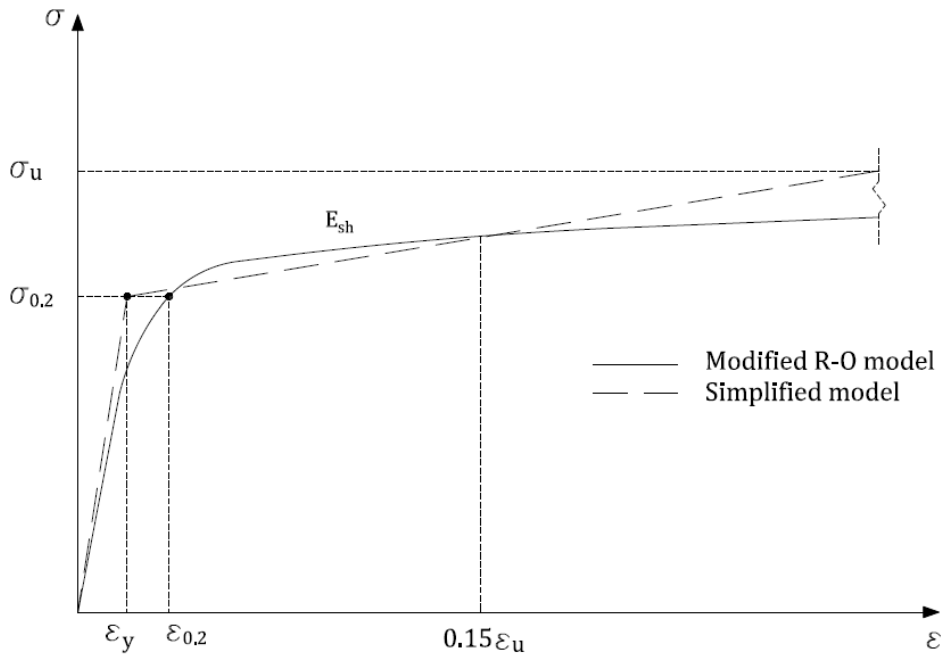

Fig. 1: The simplified and modified Ramberg-Osgood material models for stainless steel.

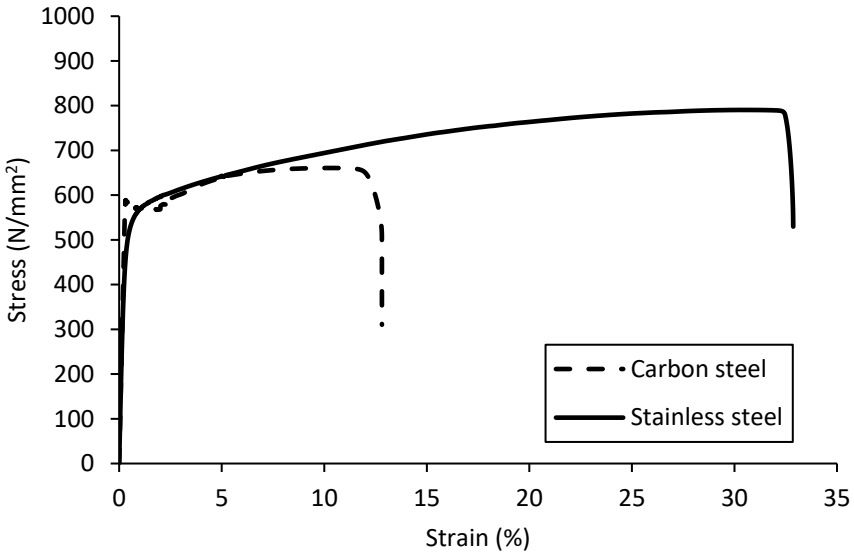

Fig. 2: Stress-strain constitutive response for stainless steel grade 1.4301 and carbon steel, with diameter of 10 mm [27].

2.2. Analytical models

The plastic bending moment capacity of the stainless steel reinforced concrete beam is obtained using either the full or simplified material models discussed in the previous section. In both of these approaches, the internal tensile and compressive forces are equated, assuming that the cross-section is in equilibrium. The internal forces are determined based on the stainless steel stress-strain material model and the equivalent rectangular compressive stress distribution in the concrete, together with the strain distribution in the section.

There are two possible cases for calculating the bending moment capacity of the section using the full and simplified material models. Case 1 is when the tensile strain of the reinforcement is less than the total strain corresponding to $\sigma_{0.2}$ (i.e. $\varepsilon \leq \varepsilon_{0.2}$ in the case of full material model and $\varepsilon \leq \varepsilon_y$ for the simplified material model) and Case 2 is when the tensile stain of the reinforcement is greater than the total strain corresponding to $\sigma_{0.2}$ (i.e. $\varepsilon > \varepsilon_{0.2}$ for the full material model and $\varepsilon > \varepsilon_y$ in the case of the simplified material model).

The stress in the reinforcement at failure of the beam is determined from the corresponding strain which is determined based on the strain distribution in the section, as follows:

$$\varepsilon = \kappa(d - y) \tag{8}$$

$$\kappa = \min(\kappa_{su}, \kappa_{cu}) \tag{9}$$

In these expressions, d is the depth of the reinforcement in the section from the top of the beam, κ is the ultimate curvature of the section, and κ_{su} and κ_{cu} are the limiting curvatures for stainless steel and concrete failures, respectively. There are two possible failure modes of the section, either crushing of the concrete (i.e. when $\kappa_{su} > \kappa_{cu}$) or by rupture of the reinforcement ($\kappa_{su} < \kappa_{cu}$). Because of the brittle nature of concrete and the high ductility of stainless steel, the failure mode of the section is dominated by crushing of the concrete in most cases. The values of κ_{su} and κ_{cu} are determined as:

$$\kappa_{su} = \frac{\varepsilon_u}{d - y}$$

$$\kappa_{cu} = \frac{\varepsilon_{cu}}{y} \tag{10}$$

The bending moment capacity of the section is obtained by firstly establishing the stress in the reinforcement and then locating the position of the neutral axis by applying equilibrium of the internal forces to the cross-section of the beam. In the case of full model, this results in complex nonlinear equations that require an iterative solution method whereas the simplified model provides a straight forward solution procedure. The full solution procedures for both methods are discussed in more detail in [24]. A flow chart presenting the full procedure for determining the neutral axis and the plastic bending moment capacity is given in Fig. 3.

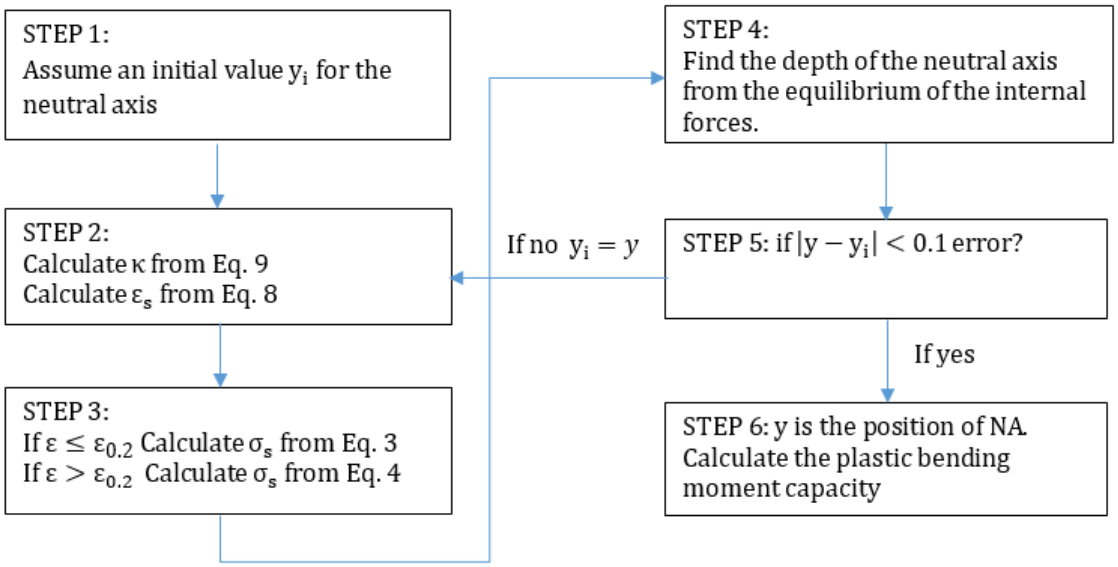

Fig. 3: Flow chart of the solution procedure for a singly reinforced concrete beam.

3. Numerical model

A finite element (FE) model has been developed using the Abaqus software [28] to simulate the behaviour of a stainless steel RC beam, with the aim of using it to examine the proposed analytical methods discussed in the previous section. This was shown to accurately predict the behaviour of reinforced concrete beams in terms of bending moment capacity, initial bending stiffness and crack propagation and patterns [24]. A similar approach is utilised herein to investigate the effect of beams geometries and materials properties of concrete and stainless steel on the structural behaviour of stainless steel RC beams, deflection at service moment and to further validate the proposed simplified model for the flexural capacity of stainless steel RC beams. In addition, in the current paper, the model is employed to conduct a detailed study into the deflection behaviour, which has not been previously considered.

The FE model is developed using an implicit dynamic solution procedure for quasi-static behaviour, which is able to achieve numerical convergence despite the nonlinearities of the behaviour. In the model, the concrete elements are represented using 3D eight-node hexahedral elements whereas the reinforcement is simulated using 2-node beam elements available in the Abaqus library [28]. The

reinforcement is embedded in the concrete and the translational degrees of freedom at each node of the reinforcement are constrained to the interpolated values of the corresponding degrees of freedom of the concrete element.

In terms of the materials, the modified Ramberg-Osgood material model described previously in Eqs. 1 and 2 is implemented to represent the behaviour of the stainless steel reinforcement. On the other hand, the nonlinear concrete behaviour in compression is modelled using Eq. 11, as given in Eurocode 2 [6]:

$$\sigma_c = \left(\frac{k\eta - \eta^2}{1 + (k-2)\eta}\right) f_{cm} \tag{11}$$

where:

$$k = 1.05E_c\frac{\varepsilon_{c1}}{f_{cm}} \qquad f_{cm} = f_{ck} + 8$$

$$\eta = \frac{\varepsilon_c}{\varepsilon_{c1}} \qquad \varepsilon_{c1}(\%) = 0.7(f_{cm})^{0.31} \leq 2.8$$

$$E_c = 22000(0.1f_{cm})^{0.3}$$

In these expressions, σ_c is the concrete compressive stress; f_{cm} and f_{ck} are the mean and characteristic values of the concrete cylinder compressive strength, respectively; ε_{c1} is the strain at the peak stress of the concrete while ε_{cu} is the ultimate strain of concrete, which is taken as 0.0035; and E_c is the Young's modulus of concrete.

The tensile stress-strain behaviour of concrete is modelled using Eq. 12, which was proposed by [29], and provides an accurate post-failure tensile response compared with linear or bi-linear relationships:

$$\begin{aligned} \sigma_t &= E_c\varepsilon_t && \text{if} \quad \varepsilon_t \leq \varepsilon_{cr} \\ \sigma_t &= f_t\left(\frac{\varepsilon_{cr}}{\varepsilon_t}\right)^{0.4} && \text{if} \quad \varepsilon_t > \varepsilon_{cr} \end{aligned} \tag{12}$$

In these expressions, ε_t is the concrete tensile strain corresponding to the tensile stress (σ_t) and ε_{cr} is the tensile cracking strain corresponding to the tensile strength of concrete (f_t), determined as:

$$f_t = 0.3(f_{ck})^{2/3} \quad (13)$$

3.1. Failure criteria

In the numerical analysis, it is typically assumed that ultimate failure of a normally reinforced concrete beam occurs when the outer fibre of the concrete in compression reaches the ultimate crushing strain (usually taken as 0.003 or 0.0035). This is likely to occur when the reinforcement material exhibits elastic perfectly-plastic stress-strain properties, because the compressive strain in the concrete at the top surface is reached after the reinforcement yields so the steel no longer contributes towards the ultimate bearing capacity of the section. However, this behaviour is different when the reinforcement is made from stainless steel rather than carbon steel, owing to the significant levels of strain hardening and ductility in the stainless steel, and the lack of a distinct yield point. Even when the concrete reaches the crushing strain at the top surface, the stainless steel reinforcement is still contributing towards the ultimate bearing capacity of the section. In addition, it is difficult to predict exactly when the concrete has crushed and therefore, it is necessary to make an assumption regarding the exact point at which the concrete is assumed to have failed (e.g. once the first node at the top surface reaches the assumed strain limit or all nodes on the top surface). In order to avoid this uncertainty, in the current work the maximum capacity of the section is taken at the ultimate load capacity of the section, in the same manner that this is commonly determined experimentally.

3.2. Validation of the FE model

The FE model has been validated using six RC beams from different experimental programmes available in the literature [30-35], three of which were reinforced with stainless steel reinforcement and three of which had traditional carbon steel reinforcement. No further experimental data on stainless steel reinforced concrete beams were available in the literature. All of the beams were tested under four-point loading conditions in displacement control. The validation includes three stainless steel RC beams, namely B3, SS and BKW1, and three other beams (SR6, U2 and O) reinforced with carbon steel reinforcement for additional robustness. The full details of the geometry and material properties for these beams are available in [24].

Fig. 4 shows the numerical load-displacement response for beams SS, SR6, U2, O and BKW1 in comparison with the corresponding experimental data. Fig. 5 presents the moment-displacement response for beam B3, since this is that manner that the experimental data is published [35]. It is observed that the model provides an excellent depiction of the experimental behaviour in all cases in terms initial stiffness, cracking point, and ultimate strength. It is found that the model slightly over-estimates the initial stiffness of the beams most likely because of some localized cracking in the experiment were not captured by the numerical model.

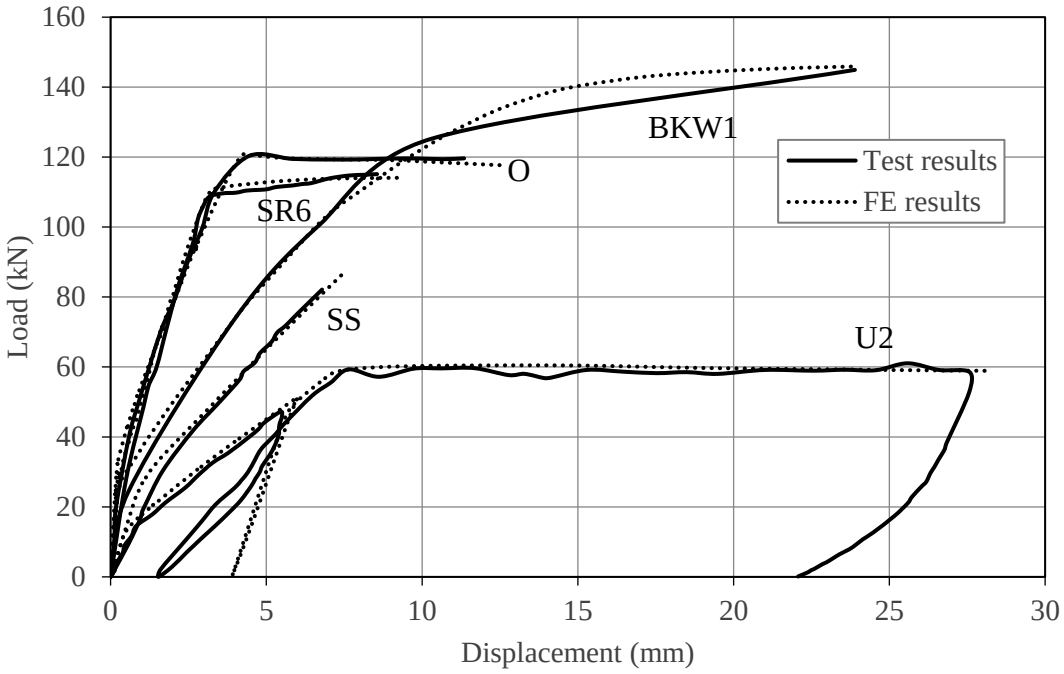

Fig. 4: Comparison between experimental and numerical load-displacement curves for beams U2 [30], O [31], SS [32], SR6 [33] and BKW1 [34].

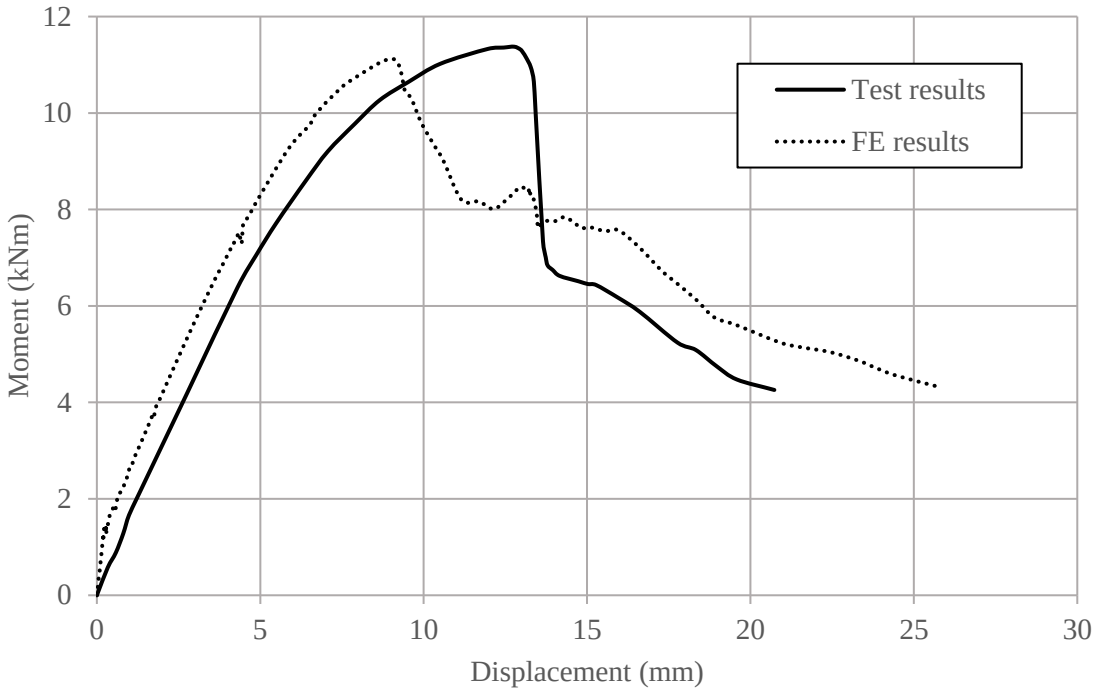

241

242 Fig. 5: Comparison between experimental and numerical moment-displacement curves for beam B3

243 [35].

244 ## 4. Analysis of the behaviour

245 In this section, the performance of stainless steel reinforced concrete beams with different geometric
246 and material properties is assessed using the FE model. Moreover, the accuracy of the proposed design
247 models is analysed against the numerical results, with reference to the current design provisions in
248 Eurocode 2. Around 200 numerical simulations have been conducted to investigate the influence that
249 the design parameters have on the exploitation of strain hardening and ductility of the stainless steel
250 reinforcement in the section, including concrete strength, grade of stainless steel, geometry and
251 reinforcement ratio. In addition, a detailed study into the influence of these parameters on the deflections
252 and the accuracy of the Eurocode 2 provisions, is also presented.

253 All of the members in this study are assumed to be simply supported beams under four-point loading
254 conditions and have a clear span of 3300 mm in order to avoid shear failure in the beam. Each member
255 has two reinforcements with diameter of 12 mm, unless it is stated otherwise. The full range of
256 parameters examined is presented in Table 1. The material data presented by [36] for these grades is

given in Table 2, including the n and m parameters required for application of the modified Ramberg-Osgood material model.

Table 1: Range of geometrical parameters included in the study.

Parameter	Range examined
Concrete grade	C20, C30, C40, C50
Grade of stainless steel reinforcement	Austenitic 1.4311, lean duplex 1.4162 and Austenitic 1.4307
Width/height (b/h) ratio of the beam	0.55 to 1
Diameter of the reinforcement	12 mm and 20 mm
Reinforcement ratio (%)	0.187 – 5.2 %

Table 2: Material properties of stainless steel reinforcement included in the study [36].

Stainless steel type	Grade	$\sigma_{0.2}$ (N/mm^2)	σ_u (N/mm^2)	E (kN/mm^2)	ε_u (%)	n	m
Austenitic	1.4311 (304LN)	480	764	202.6	38.6	4.7	4.8
Lean duplex	1. 4162 (LDX2101)	682	874	199.1	20.4	5.3	5.0
Austenitic	1.4307 (304L)	562	796	210.2	30.7	4.7	4.8

4.1. Bending moment capacity predictions

Figs. 6, 7 and 8 present the bending moment predictions obtained from the proposed full analytical model (AM), the simplified analytical model (SM) and the numerical model (FE) as well as those obtained using the design method provided in Eurocode 2 (i.e. elastic-perfectly-plastic behaviour of the material is assumed), for beams reinforced with stainless steel grades 1.4311, 1.4162, 1.4307,

respectively. The results are presented in terms of bending moment versus concrete strength (f_c), to highlight how this parameter influences the behaviour.

The figures show a good agreement between the results obtained numerically with those calculated using the full proposed analytical model with average and maximum AM/FE values being -14.9% and -22.3% whilst these same values obtained using the Eurocode 2 design rules (i.e. EC2/FE) are -28.3% 23 and -44.7%, respectively. It is noteworthy that a negative value for the AM/FE ratio indicates a conservative result from the analytical model. Clearly, the Eurocode 2 design rules provide an overly conservative prediction of the ultimate bending moment capacity, whereas the full analytical design model provides less conservative yet accurate and reasonably realistic results. There are still some disparities between the analytical and numerical results, which are most likely owing to some of the simplifications in the analytical model. These include the assumption that concrete does not contribute to the load carrying capacity in tension and also the idealisation of rectangular stress blocks. Nevertheless, the results are better than the existing design provisions, and remain on the conservative side consistently.

The simplified analytical model which incorporates the bilinear stress-strain curve for the stainless steel, also provides conservative predictions for the bending moment capacity in most cases with the average and maximum SM/FE values being -9.9% and -26.8%, respectively. It is noteworthy that the simplified analytical model provides less conservative results overall compared with the full analytical model mainly because the simplified material model has a greater slope in the strain hardening region. In addition, in a small number of cases when beams have a relatively low b/h ratio and are made using high strength concrete and grade 1.4162 stainless steel, the simplified analytical model tends to overestimate the bending moment capacity compared with the numerical results, which slightly skews the average and maximum SM/FE values given before. Therefore, it is necessary to recalibrate the simplified method in order to achieve better agreement with full method predictions, and to provide conservative predictions for all cases, as discussed in the following section.

4.1.1. Proposed modifications into the simplified analytical model

In this section, the slope of the strain hardening portion of the stainless steel constitutive relationship is modified to improve the accuracy of the simplified analytical model, especially for the cases highlighted in the previous section where slightly unconservative results were obtained. This is achieved by recalibrating the C_2 parameter in Eq. 7 based on the extensive range of numerical data obtained. Since different stainless steel grades have their own mechanical properties, an optimization study for the C_2 parameter is conducted individually for each material type. Consequently, it has been found that the most accurate bending moment predictions for the full range of parameters examined in the current study are achieved using a C_2 value of 0.25 for beams with austenitic stainless steel grades 1.4311 and 1.4307, and 0.3 for beams with lean duplex stainless steel grade 1.4162. This is reasonably acceptable as a higher value of C_2 results in a lower E_{sh} value and hence lower strain hardening capacity, as is the case for lean duplex stainless steel compared with the austenitic grades.

The results of the simplified analytical model predicted using the new proposed values for C_2 (denoted as SM-I) are presented in Figs. 6, 7 and 8, for beams made using grade 1.4311, 1.4162 and 1.4307 stainless steel, respectively. The figure also presents the data from the previous C_2 value of 0.15 (SM in the figures). It is observed that the simplified analytical model predictions with the newly proposed C_2 values are in excellent agreement with the predictions of the full analytical model. The average and maximum SM-I/AM ratios are -2.8% and -17.2%, respectively, whilst these same values for SM/AM are 5.9% and 34.5%, respectively. This also ensures that the simplified predictions are below that of the numerical model, for all examined cases. Therefore, the proposed values for C_2 parameter are implemented in the simplified analytical model for all the results presented in the following sections.

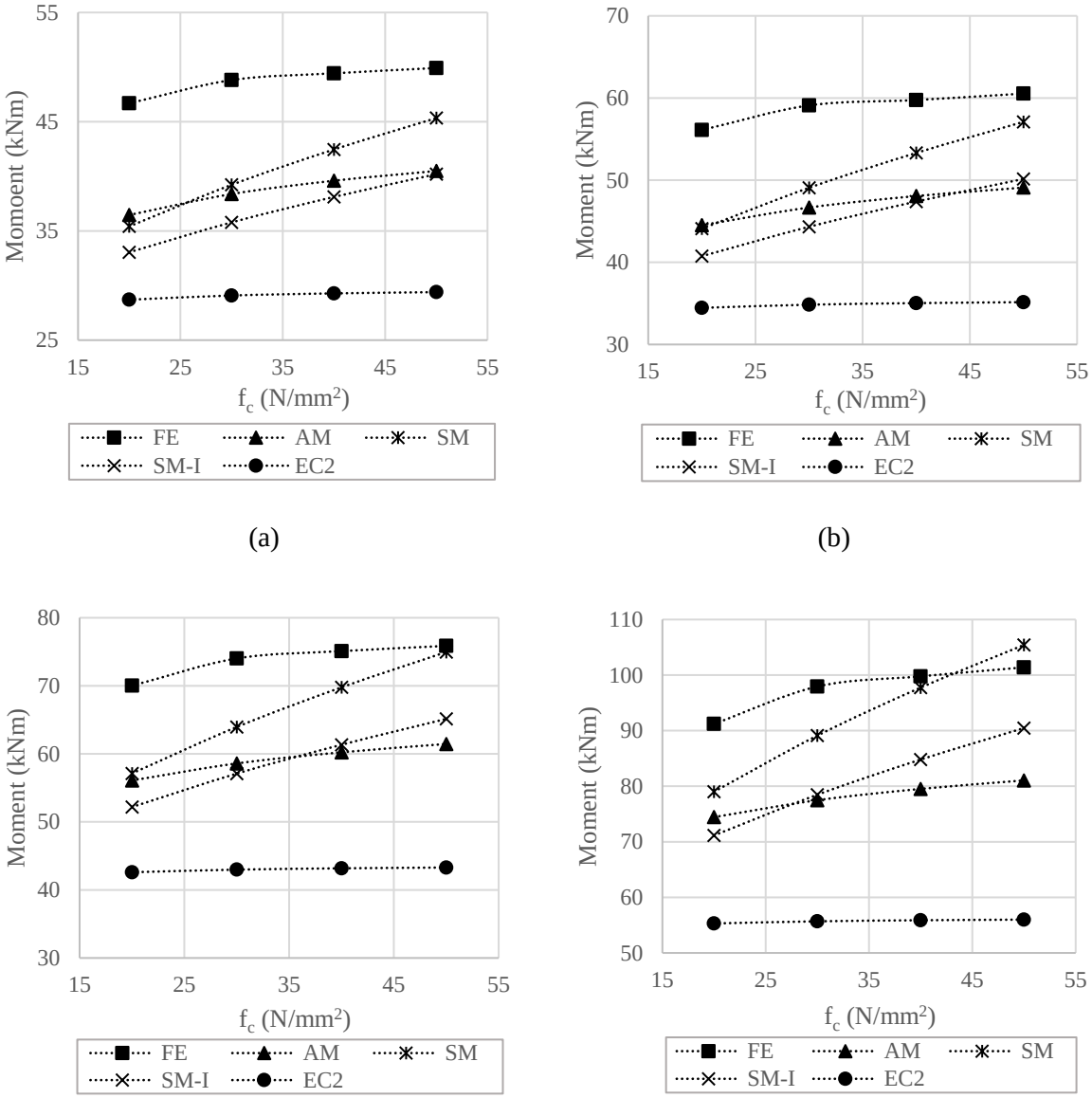

313 Fig. 6: Bending moment predictions for beams with grade 1.4311 austenitic stainless steel using a b/h

314 ratio of (a) 1.00 (b) 0.85 (c) 0.70 and (d) 0.55.

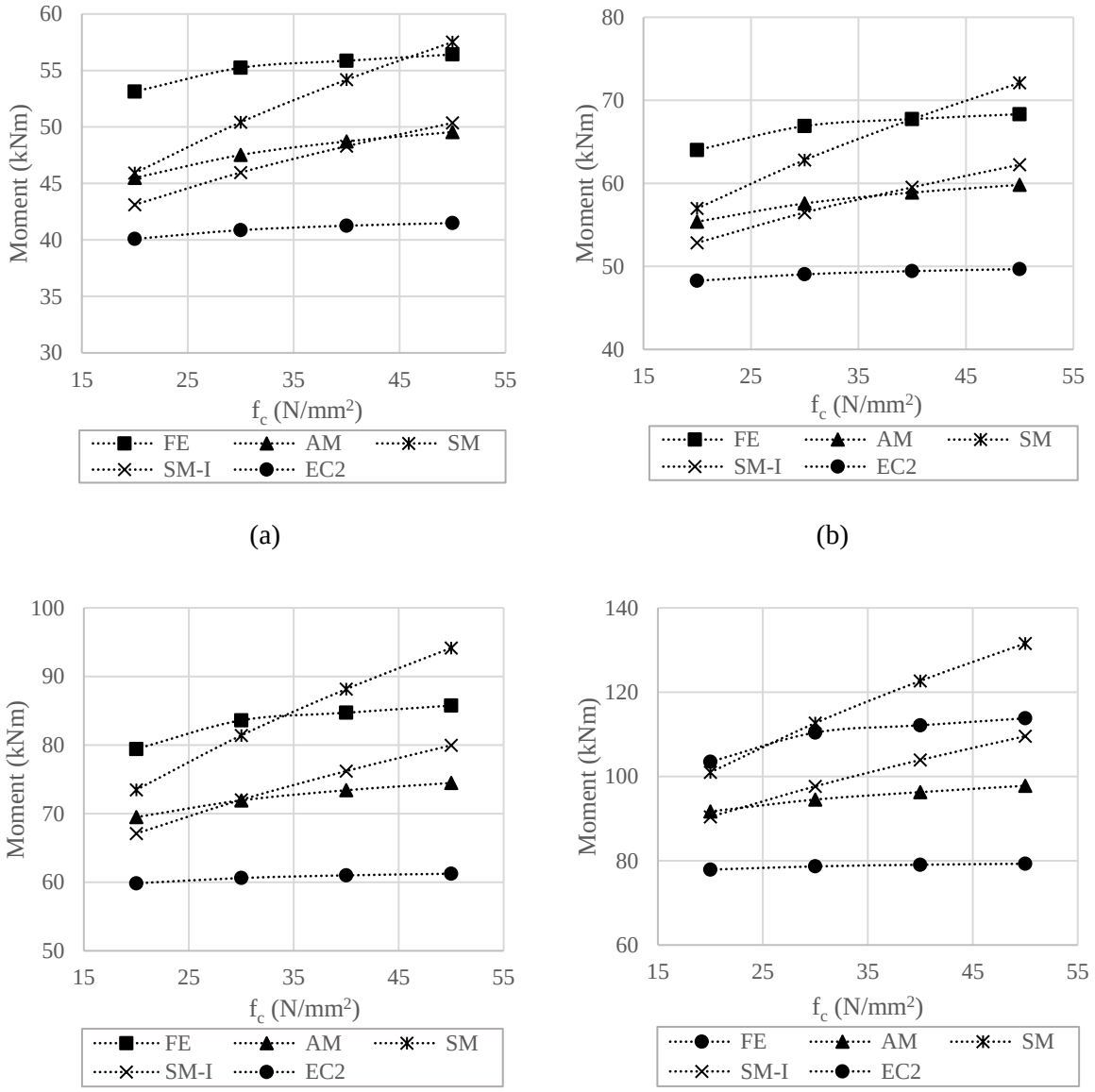

315 Fig. 7: Bending moment predictions for beams with grade 1.4162 duplex stainless steel using a b/h

316 ratio of (a) 1.00 (b) 0.85 (c) 0.70 and (d) 0.55.

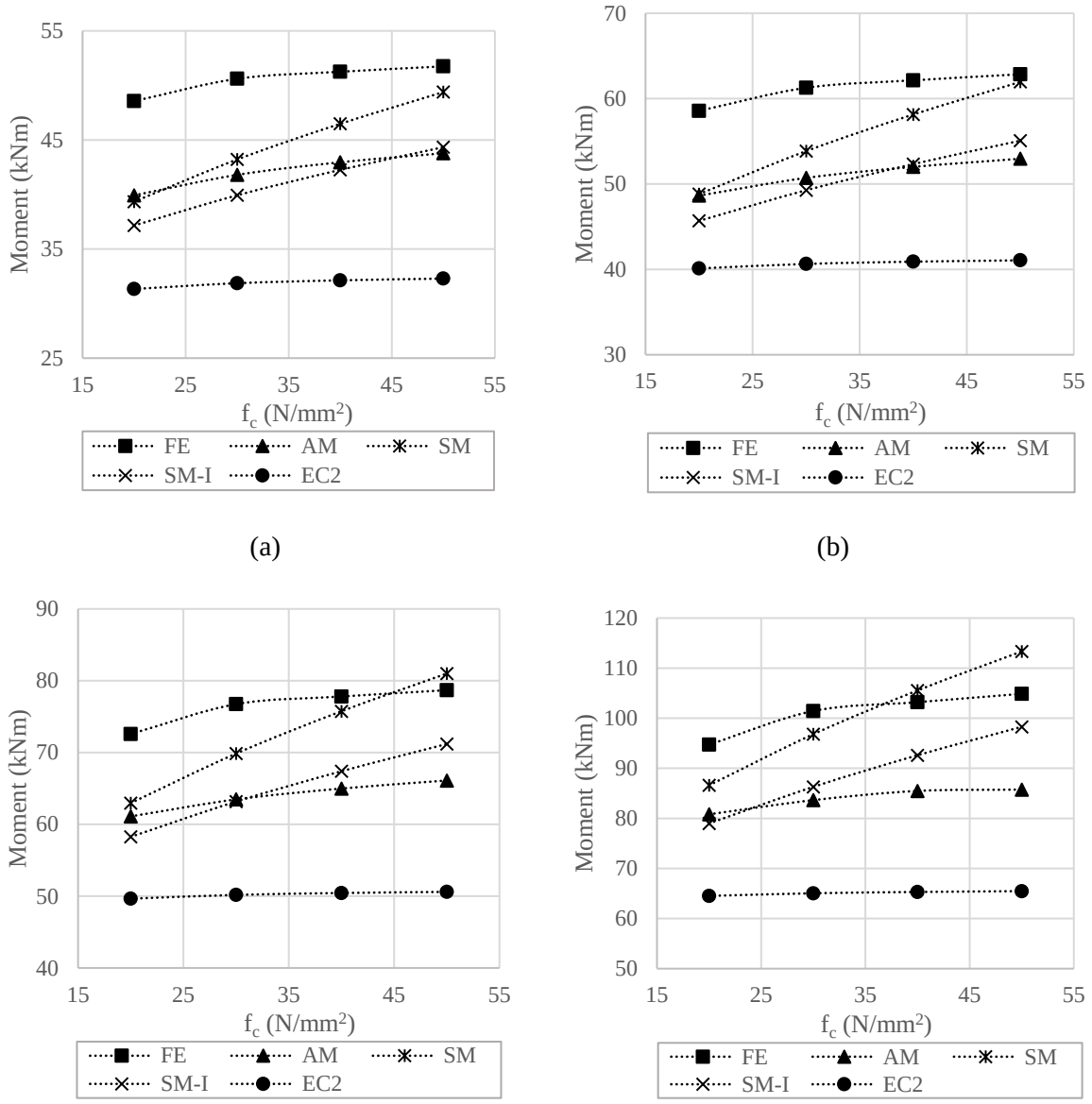

317 Fig. 8: Bending moment predictions for beams with grade 1.4307 austenitic stainless steel using a b/h
318 ratio of (a) 1.00 (b) 0.85 (c) 0.7 and (d) 0.55.

319 4.2. Influence of concrete strength

320 The results presented in Figs. 6, 7 and 8 exhibit the influence that concrete strength has on the ultimate
321 bending moment capacity for a range of beam geometries and different grades of stainless steel. It is
322 observed that the ultimate bending moment capacity obtained using the numerical model and the full
323 analytical model improves by around 8% on average, respectively, when the concrete strength is
324 increased from 20 to 50 MPa, for all cases considered. Whilst this same value for the simplified

analytical model is 21.5%. Clearly, the ultimate bending moment calculated from the simplified analytical model is more influenced by the strength of concrete compared with those obtained using the numerical or the full analytical models. This is perhaps owing to the simplified bi-linear material behaviour of the stainless steel employed in the simplified material model which, for beams made from a relatively higher concrete strength, enables the reinforcement to carry further tensile forces prior concrete crushing failure. Despite this, all the predictions of the simplified method are currently lower than the numerical values, considering the new proposed values for the C_2 parameter.

The effect of concrete strength on the load-displacement response is illustrated in Figs. 9, 10 and 11 for beams made using stainless steel reinforcement in grade 1.4311, 1.4162 and 1.4307, respectively. The section used in this analysis is 300 mm in width and 545 mm in height (i.e. the b/h ratio is 0.55). The concrete strength is varied between 20 and 50 MPa. It is clear that as expected, the initial bending stiffness, crack load (i.e. identified as the load in which the slope of the load-displacement curve begins to change) and ultimate load of the beam is improved by increasing the strength of concrete, for all cases. For example, increasing the strength of concrete from 20 MPa to 50 MPa enhances the cracking load and the ultimate load by around 43% and 11% on average, respectively. Beams with C20 concrete exhibit a softer bending stiffness, lower cracking load and ultimate load compared with the responses obtained using the other concrete strengths. This is most likely because the lower tensile strength of C20 leads to greater cracking in the specimen which affects the overall load-displacement response.

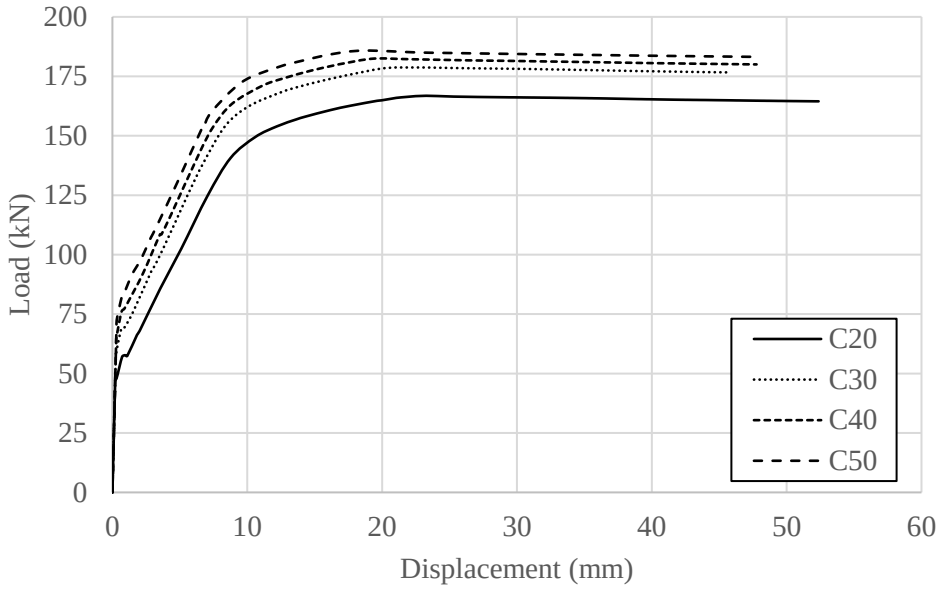

343

344 Fig. 9: Load-displacement curves obtained numerically using various concrete strength for beams

345 with stainless steel grade 1.4311.

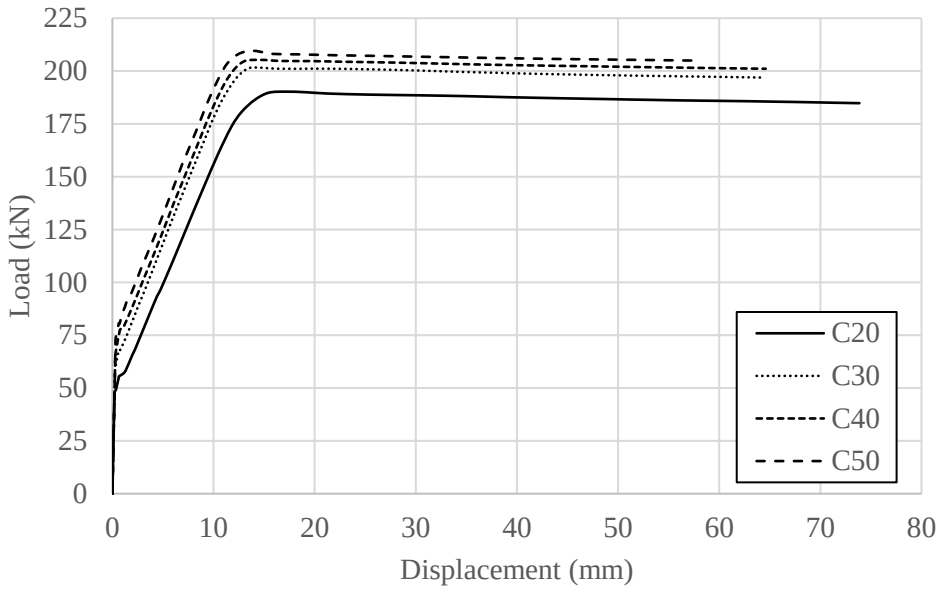

346

347 Fig. 10: Load-displacement curves obtained numerically using various concrete strength for beams

348 with stainless steel grade 1.4162.

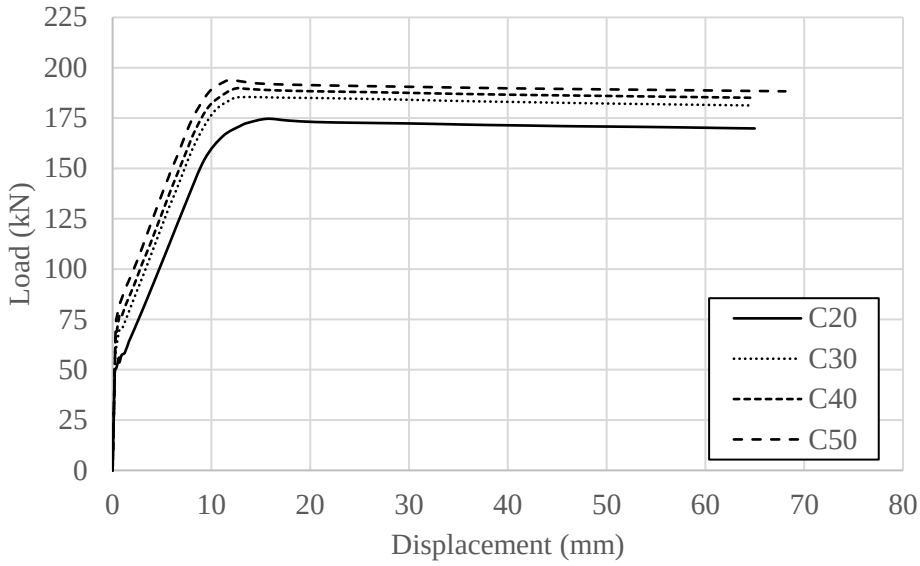

Fig. 11: Load-displacement curves obtained numerically using various concrete strength for beams with stainless steel grade 1.4307.

4.3. Stainless steel grade

The effect that stainless steel grade has on the load-displacement response is illustrated in Fig. 12. For illustrative purposes, a beam with C50 concrete is considered in this study which is 300 mm in width and 545 mm in height (i.e. b/h ratio of 0.55). It is evident from the figure that using different stainless steel grades shows no significant effect on the cracking load or the initial bending stiffness of the beams mainly owing to having similar modulus of elasticity. However, using stainless steel grades 1.4162 and 1.4307 improves the ultimate load capacity by around 13% and 4%, respectively, compared to grade 1.4311. It is noteworthy that grade 1.4162 has the highest yield strength of the grades examined in this study, and therefore the beam with reinforcement made from this material is expected to reach a higher load capacity.

Fig. 12 also shows the load-displacement response for a similar beam with carbon steel reinforcement. It is assumed that the carbon steel material model is elastic-perfectly plastic, in accordance with the guidance given in Eurocode 2 [6]. Although there are likely to be some deviations between the real stress-strain behaviour of carbon steel reinforcement and this bilinear model, the model is generally a good representation of the carbon steel constitutive response, as shown in Fig. 2. The modulus of

elasticity and yield strength are taken as 200 GPa and 500 N/mm^2, respectively. The figure illustrates that using carbon steel reinforcement shows no considerable difference in terms of the cracking load or the initial bending stiffness of the beams, compared with the stainless steel reinforced concrete members. However, it is clearly observed that the ultimate load capacity for the beam with carbon steel rebars is significantly lower, by around 27% on average, compared with that of stainless steel beams. Additionally, it is evident from Table 3 that beams with carbon steel reinforcement develop lower ultimate bending moment capacities compared with those of stainless steel beams.

The other important observation is that the deflection at the ultimate load of the beam is influenced by the grade of stainless steel, as shown in Fig. 12. For instance, the beam with grade 1.4311 stainless steel reinforcement deflects to 18.6 mm at the ultimate load whereas the corresponding deflections for beams with grades 1.4162 and 1.4307 are 13.4 and 12 mm, respectively. Given that grade 1.4311 has the highest strain hardening capacity of the stainless steels examined herein, it is clearly intuitive to conclude that the ductility of the section is improved by using reinforcement with a greater ultimate strain.

In order to analyse the accuracy of the full and simplified analytical models when different stainless steel grades are used, Table 3 shows a comparison of the bending moment predictions obtained numerically and analytically with reference to the predictions of Eurocode 2. The results are obtained for two different sections with width to height (b/h) ratios of 0.55 and 0.70. The results demonstrate that both the full and simplified models as well as the Eurocode 2 tend to provide less conservative bending moment predictions compared with the numerical values when a grade of stainless steel with a relatively higher strength is used.

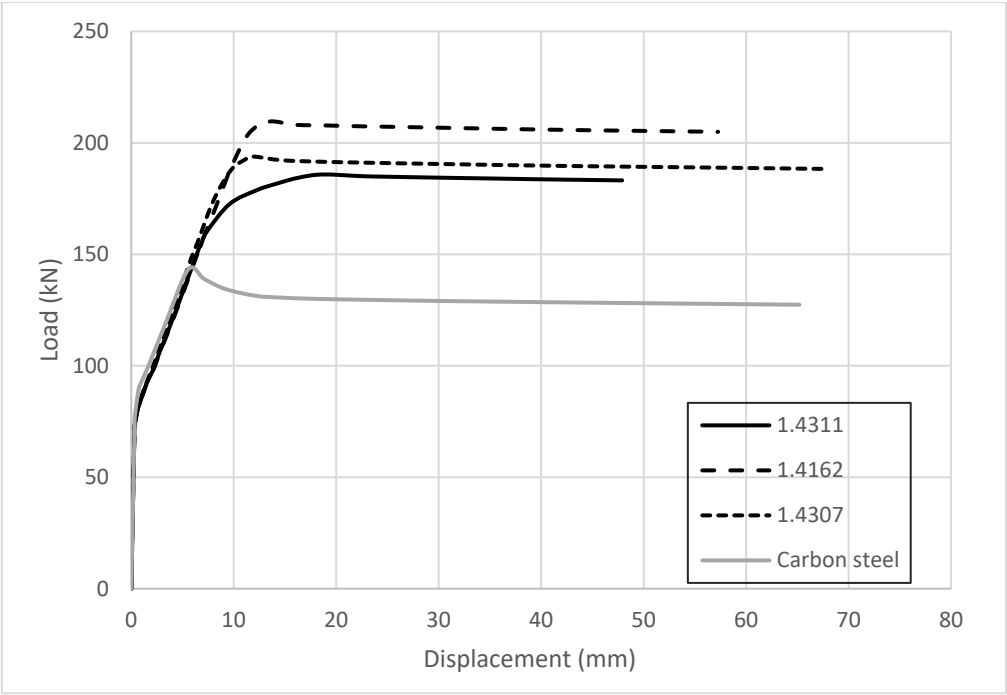

389

390 Fig. 12: Load-displacement curves obtained numerically for different reinforcement grades.

391 Table 3: Comparison between the ultimate bending moment predictions obtained numerically and

392 analytically for different reinforcement grades.

b/h ratio	Grade	FE (kNm)	AM (kNm)	SM-I (kNm)	EC2 (kNm)	AM/FE %	SM-I/FE %	EC2/FE %
0.55	1.4311	101.4	81.0	90.5	56.0	-20.1	-10.8	-44.8
	1.4162	113.8	97.8	109.5	79.3	-14.1	-3.7	-30.3
	1.4307	104.9	85.8	98.3	65.5	-18.2	-6.3	-37.6
	B500b	78.9	-	-	58.3	-	-	-26.1
0.7	1.4311	75.9	61.4	65.1	43.3	-19.0	-14.1	-42.9
	1.4162	85.8	74.5	80.0	61.2	-13.2	-6.8	-28.6
	1.4307	78.7	66.1	71.2	50.6	-16.0	-9.5	-35.7
	B500b	56.4	-	-	45.14	-	-	-20

393

4.4. Geometry

In order to investigate the effect that the geometry of the section has on the behaviour of stainless steel RC beams, beams with different b/h ratios ranging from 1.00 to 0.55 are considered in the current section. The results presented are obtained for beams made from C50 concrete. Figs. 13, 14 and 15 illustrate the relationship between the bending moment predictions obtained from the numerical and analytical models, and b/h ratios for beams with stainless steel grades 1.4311, 1.4162 and 1.4307, respectively. It is clear that the ultimate bending moment significantly increases for beams with a relatively lower b/h ratio, as expected since these beams would have a greater second moment of area. The simplified analytical model tends to provide a higher prediction compared with the full analytical model for beams with a lower b/h ratio. However, the bending moment predictions obtained from the simplified analytical model are lower than those obtained numerically in all cases, therefore providing a conservative prediction. It is noteworthy that the full analytical method improves the accuracy of the bending capacity of the section by around 41%, 21% and 32% on average, compared with the current design approach in Eurocode 2, for the results presented in this section and obtained using stainless steel grades 1.4311, 1.4162 and 1.4307, respectively.

Fig. 16 presents the relationship between the beam geometry and the ability of the section to exploit the strain hardening capabilities of the stainless steel, using the full analytical model. It is shown that the geometry of the beam has a relatively small influence on the exploitation of strain hardening. For example, a beam with a b/h ratio of 0.55 develops around 4.2%, 2.9% and 2.2% more stress in the reinforcement for grades 1.4311, 1.4162 and 1.4307, respectively, compared with members with a b/h ratio of 1.00. In general, it is observed that beams reinforced with 1.4162 grade lean duplex stainless steel reinforcement exhibit greater exploitation of the strain hardening capacity in the stainless steel, compared with beams reinforced with the austenitic grades 1.4307 and 1.4311.

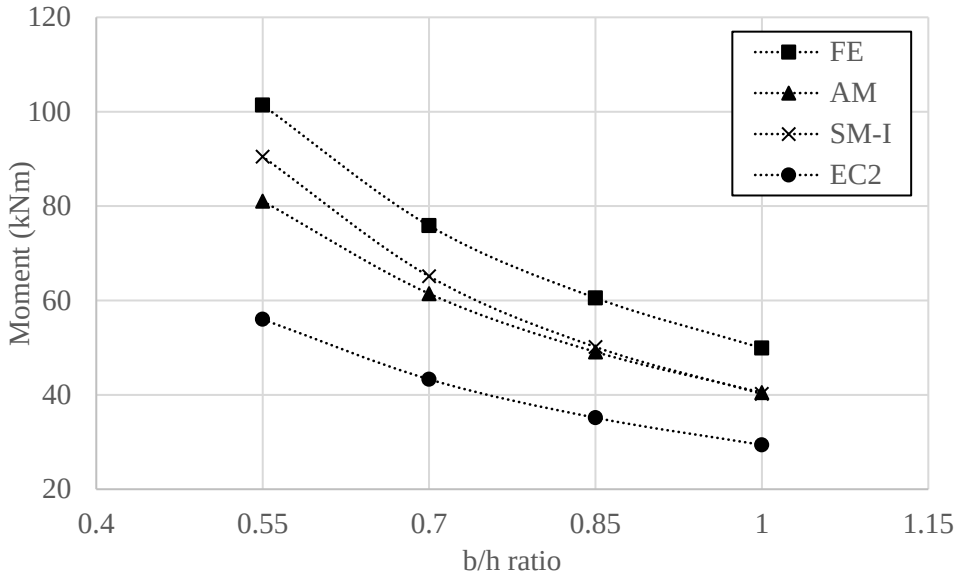

417

418 Fig. 13: Effect of the beam geometry on the bending moment predictions for beams with austenitic

419 stainless steel grade 1.4311.

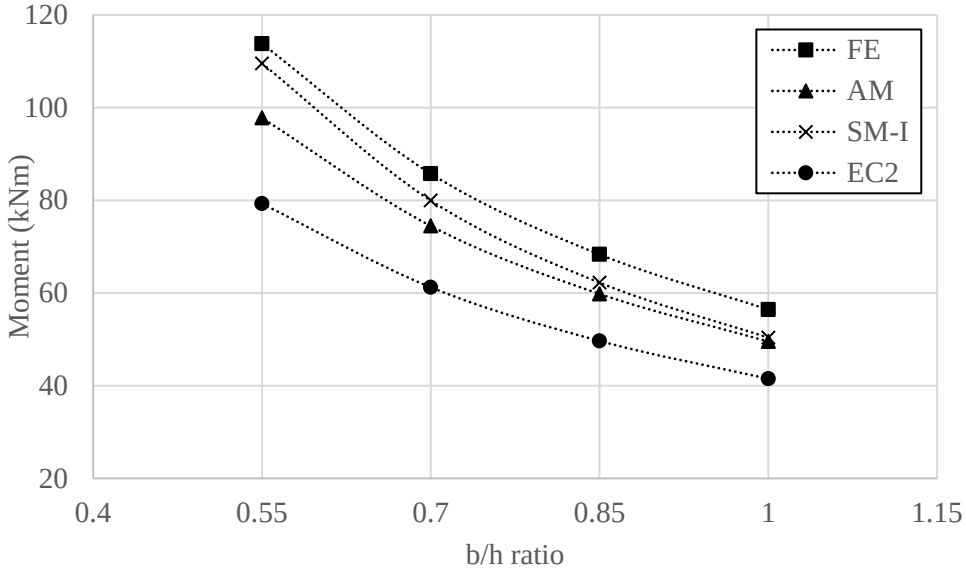

420

421 Fig. 14: Effect of the beam geometry on the bending moment predictions for beams with lean duplex

422 stainless steel grade 1.4162

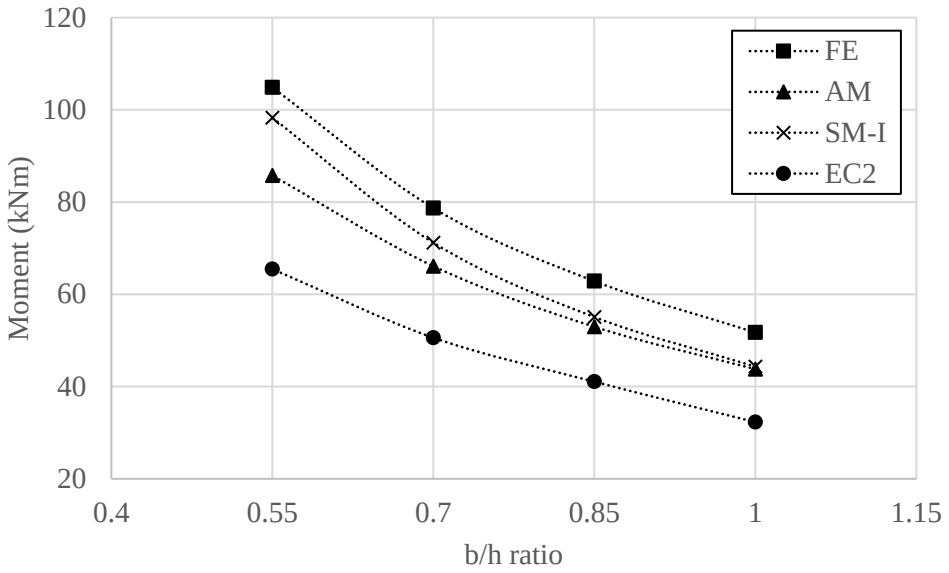

Fig. 15: Effect of the beam geometry on the bending moment predictions for beams with austenitic stainless steel grade 1.4307.

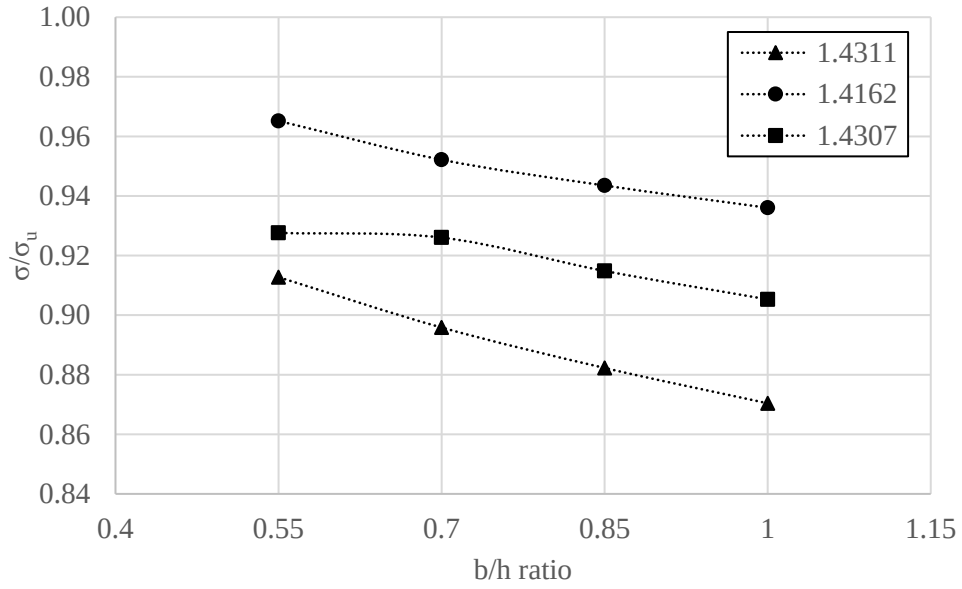

Fig. 16: Effect of the beam geometry on the exploitation of strain hardening.

4.5. Reinforcement ratio

Reinforcement ratio is an important parameter in the design of reinforced concrete sections as it dictates not only the load carrying capacity but also the failure mode. In this section, the influence of reinforcement ratio on the behaviour of stainless steel RC beams, in particular the exploitation of strain

hardening in the reinforcement, is assessed. The results presented are obtained for beams with concrete strength C40 and a b/h ratio of 0.70.

Figs. 17, 18 and 19 illustrate the effect that reinforcement ratio (ρ) has on the bending moment capacity values obtained numerically and analytically for beams made using stainless steel reinforcement in grades 1.4311, 1.4162 and 1.4307, respectively. The results demonstrate that both the full and simplified analytical models underestimate the bending moment capacities obtained numerically in almost all cases, which is conservative and in line with previous findings. The numerical analyses show that the bending moment capacity improves as the reinforcement ratio increases until it reaches a specific ratio (i.e. around 0.032 in the cases presented herein) after which no further improvement in the bending capacity is observed. The reason for this is most likely due to the greater depth of the neutral axis when a higher reinforcement ratio is employed which increases the compressive stress in the concrete until it crushes, and no further improvement can be achieved. Moreover, both the simplified analytical model and the Eurocode 2 design rules provide identical predictions, as expected, when a higher reinforcement ratio is used since both models are based on the same constitutive behaviour for the stainless steel in the elastic range. It is also observed that for beams with a relatively higher reinforcement ratio, the moment capacities predicted by the full analytical model are below those from the simplified analytical model and also Eurocode 2. This is owing to the nonlinearity of the material model which starts from an early stage.

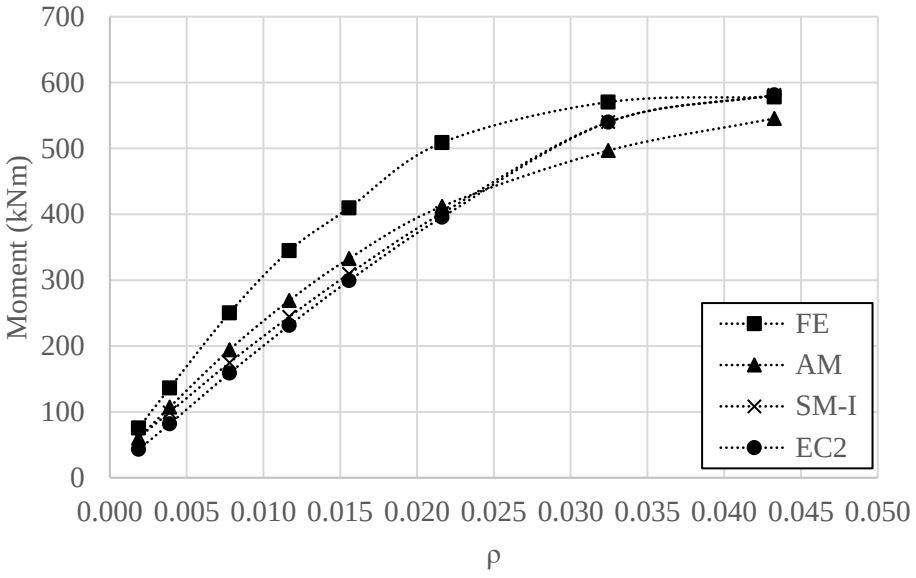

Fig. 17: Effect of the reinforcement ratio (ρ) on the bending moment capacity for beams made using grade 1.4311 austenitic stainless steel.

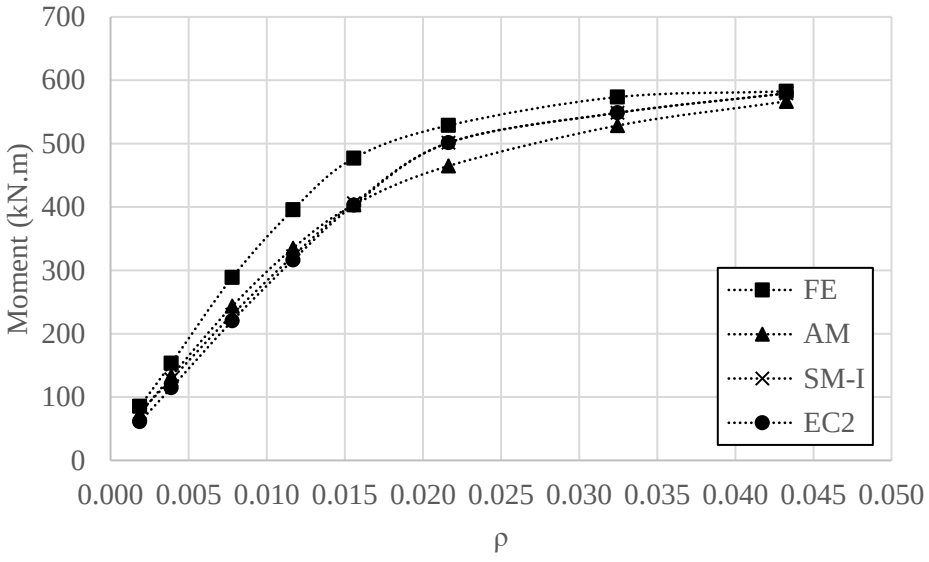

Fig. 18: Effect of the reinforcement ratio (ρ) on the bending moment capacity for beams made using grade 1.4162 lean duplex stainless steel.

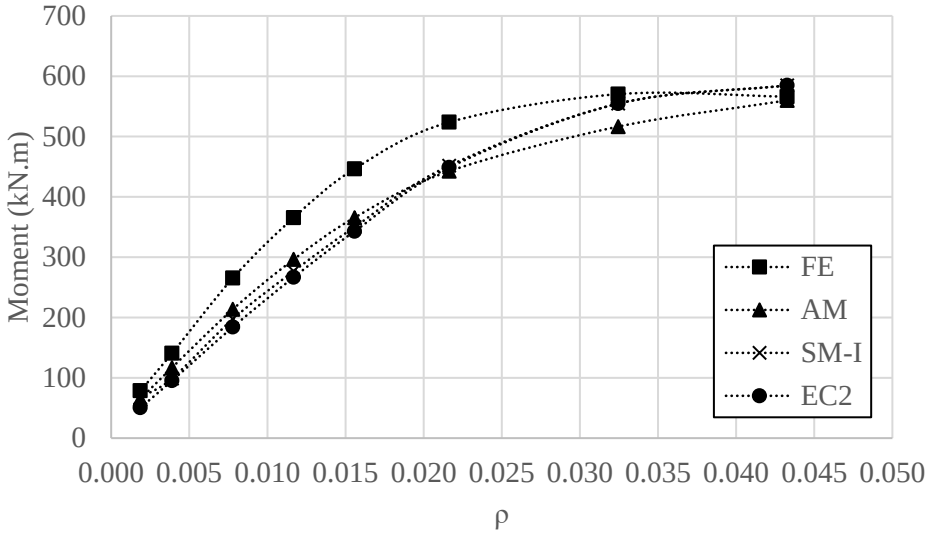

Fig. 19: Effect of the reinforcement ratio (ρ) on the bending moment capacity for beams made using grade 1.4307 austenitic stainless steel.

Figs. 20, 21 and 22 demonstrate the influence of reinforcement ratio on the exploitation of strain hardening in the rebar for beams with stainless steel reinforcement in grades 1.4311, 1.4162 and 1.4307, respectively. These results are obtained using the full analytical model, for a range of different concrete strengths. The figures illustrate the amount of stress in the rebars that can be exploited when calculating the ultimate bending moment capacity of the section. The horizontal solid line in each of the figures represents the yield limit for that particular grade of stainless steel (i.e. $\sigma_{0.2}/\sigma_u$).

It is shown in the figures that further exploitation of the strain hardening capacity in the reinforcement is achieved when a relatively higher grade of concrete is employed. This is mainly because the higher strength concrete can carry greater compressive forces allowing the rebar to reach greater levels of stress. In all cases, it is observed that the level of stress in the stainless steel is relatively lower when a higher reinforcement ratio is employed. This is because an increase in the steel cross-sectional area generally reduces the levels of stress and strain in the reinforcement and increases the depth of the neutral axis, which causes a relative increase in the levels of applied stress and strain in the concrete resulting in crushing of the concrete. Accordingly, lower exploitation of the tensile strength in the reinforcement is achieved.

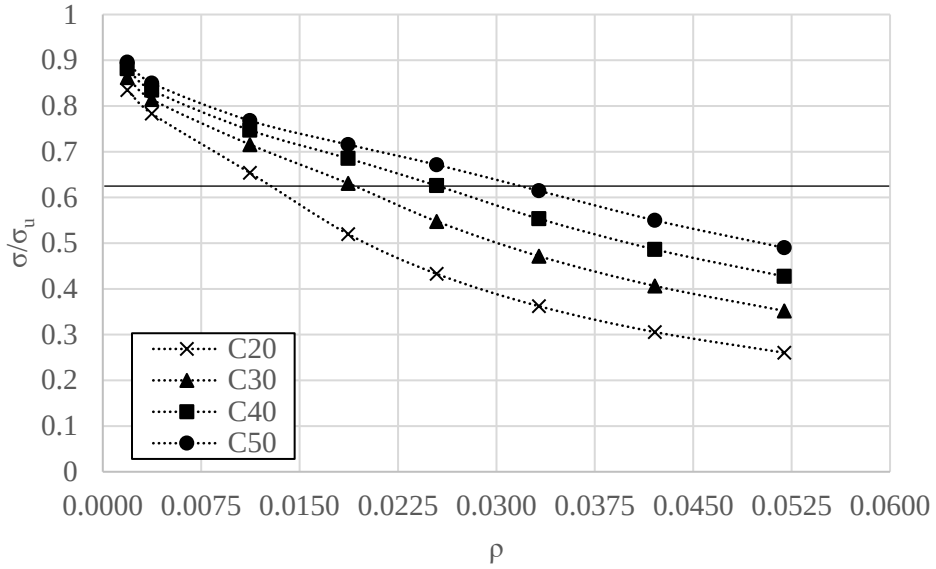

474

475 Fig. 20: Effect of reinforcement ratio on the exploitation of strain hardening for beams reinforced with

476 grade 1.4311 austenitic stainless steel.

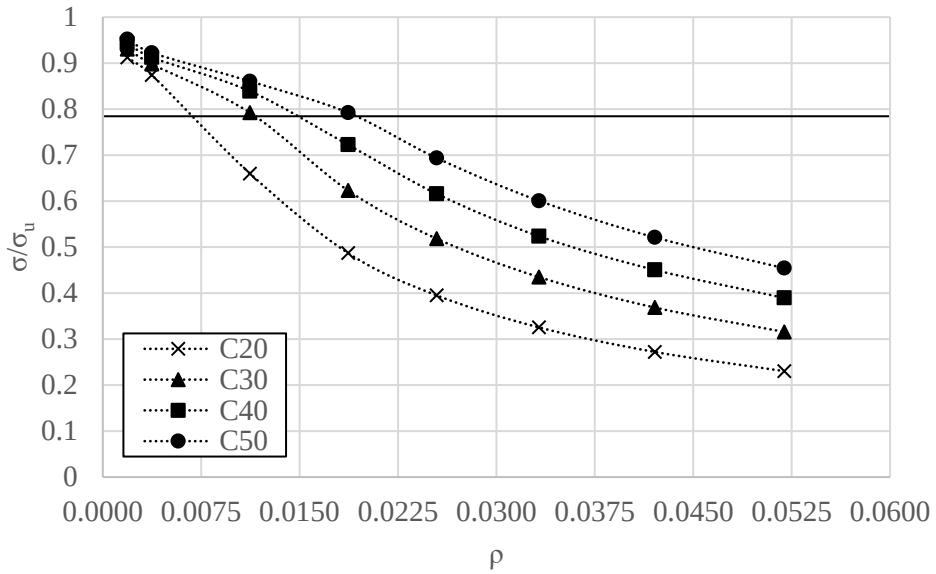

477

478 Fig. 21: Effect of reinforcement ratio on the exploitation of strain hardening for beams reinforced with

479 grade 1.4162 lean duplex stainless steel.

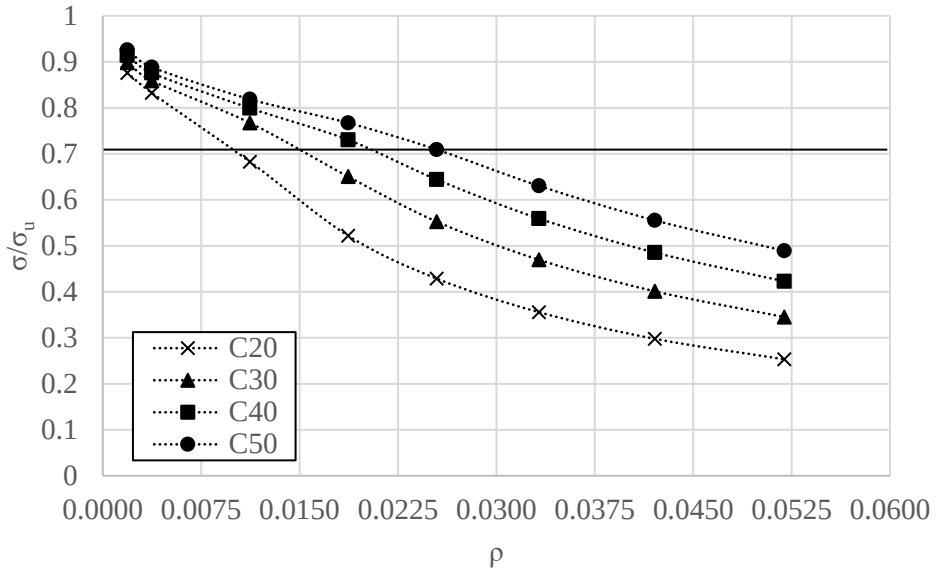

480

481 Fig. 22: Effect of reinforcement ratio on the exploitation of strain hardening for beams reinforced with
482 grade 1.4307 austenitic stainless steel.

483 A balanced reinforcement ratio (ρ_{bal}) is defined in this paper as the ratio where concrete crushing and
484 reinforcement yielding occur simultaneously in the cross section. In order to utilize and exploit the
485 positive strain hardening properties of stainless steel reinforcement in the design of reinforced concrete
486 beams, it is necessary to design the section to be under-reinforced. An under-reinforced section is when
487 the reinforcement ratio is lower than the balanced ratio (i.e. $\rho < \rho_{bal}$). This allows the reinforcement to
488 yield first and then develop some strain hardening before the section fails due to crushing of concrete.
489 It ensures enough ductility in the section to avoid sudden catastrophic failure of the reinforced concrete
490 member. On the other hand, if the beam is designed to be over-reinforced (i.e. $\rho > \rho_{bal}$), failure will
491 occur by crushing of the concrete before the rebar yields, and the strain hardening characteristics of the
492 stainless steel will not be exploited. This design case is neither desirable nor efficient, but could still be
493 employed if a higher partial safety factor is considered.

494 A balanced reinforcement ratio (ρ_{bal}) can be identified for stainless steel reinforced concrete sections as
495 the reinforcement ratio at which when the tensile strain in the rebar reaches to 0.2% strain ($\varepsilon_{0.2}$)
496 simultaneously with the concrete on the top surface reaching the ultimate crushing strain (ε_{cu}). This

requires obtaining the depth of the neutral axis (y) from the strain distribution in Fig. 23, as presented in Eq. 14:

$$y = \frac{d}{1 + \varepsilon_{0.2}/\varepsilon_{cu}} \tag{14}$$

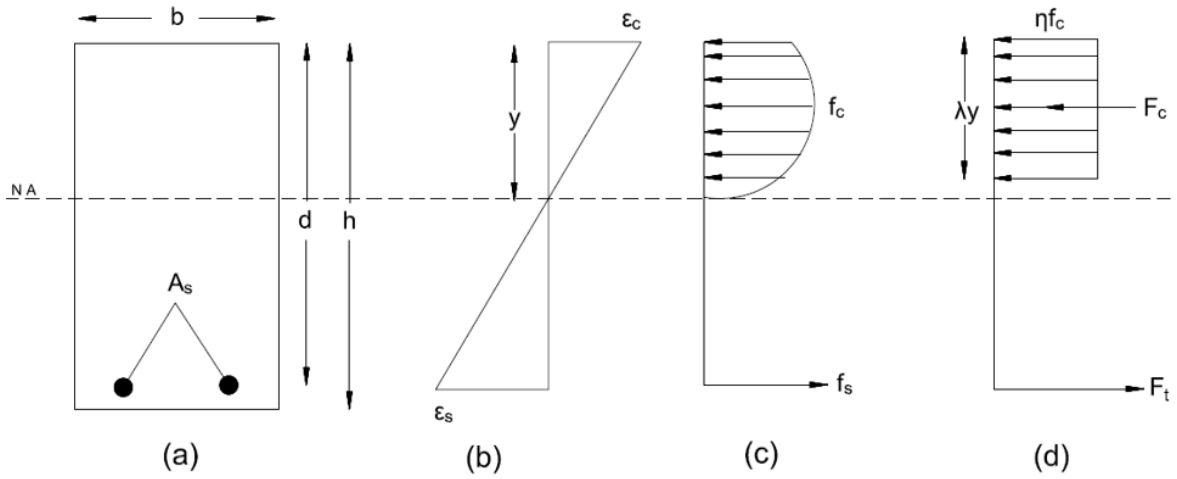

Fig. 23: Strain and stress distribution diagrams for a reinforced concrete beam including (a) the cross-section (b) the strain distribution, (c) the stress distribution and (d) an equivalent stress distribution in the section.

The equilibrium of internal forces can be applied, as presented in Eq. 15, by assuming the depth of the compressive stress block of the concrete is 0.8y and the concrete compressive stress in the concrete stress block is $0.85f_c$:

$$0.68f_c y\, b - A_s\sigma_s = 0 \tag{15}$$

In this expression, the tensile stress (σ_s) is the 0.2% proof stress of the reinforcement ($\sigma_{0.2}$).

By substituting Eq. 14 into Eq. 15, Eq. 16 is obtained:

$$0.68f_c \left(\frac{d}{1+\varepsilon_{0.2}/\varepsilon_{cu}}\right) b - A_s\sigma_{0.2} = 0 \tag{16}$$

The balanced reinforcement ratio (ρ_{bal}) is obtained by rearranging Eq. 16, as follows:

$$\rho_{bal} = \frac{A_s}{bd} = \frac{0.68}{\sigma_{0.2}}\left(\frac{f_c}{1+\varepsilon_{0.2}/\varepsilon_{cu}}\right) \quad (17)$$

In the case of under-reinforced section, the reinforcement ratio must be greater than the minimum ratio required to prevent the rupture of the rebar which it can be obtained using Eq. 18.

$$\rho_{min} = \frac{0.68}{\sigma_u}\left(\frac{f_c}{1+\varepsilon_u/\varepsilon_{cu}}\right) \quad (18)$$

4.6. Deflections

A realistic estimation of the levels of deflection that develop in a structure is imperative to ensure acceptable serviceability and the comfort of end-users. Thus, global design standards typically provide limiting values for deflections which should not be exceeded. In Eurocode 2, for example, the allowable deflection is limited to span/250 for members subjected to quasi-permanent loads [6]. Deflections are in important consideration for concrete members reinforced with stainless steel owing to the excellent ductility of the reinforcing material. In the deflection calculations for RC beams, using the elastic modulus of stainless steel may result in over-conservative predictions due to the non-linear behaviour of the stainless steel, even in the low-strain range. Therefore, this section aims to evaluate the deflection design approach in Eurocode 2 for stainless steels RC beams. The predicted results from Eurocode 2 are compared with the corresponding values from the numerical model. The influences of implementing the secant modulus and the tangent modulus of stainless steel in the deflection calculations for RC beams are also explored.

In Eurocode 2, the deflection of a member is obtained based on the assumption that the concrete member comprises cracked and un-cracked sections, at the service load. Accordingly, the maximum deflection (δ_{EC2}) for RC members is calculated as follows:

$$\delta_{EC2} = (1-\zeta)\delta_1 + \zeta\delta_2 \quad (19)$$

In this expression, ζ is a distribution coefficient representing the tension stiffening phenomenon in the section, and is taken as zero for the un-cracked portion of the section, otherwise it is calculated using Eq. 20:

$$\zeta = 1 - \beta\left(\frac{M_{cr}}{M_a}\right)^2 \quad (20)$$

where β is a coefficient that accounts for the effect of the duration of loading on the average strain, and is assumed to have a value of unity for a single short-term loading and 0.5 for sustained and cyclic loading. M_{cr} and M_a are the bending moment values calculated at the cracking and service loads, respectively. The cracking moment (M_{cr}) is determined as:

$$M_{cr} = \frac{f_t I_g}{y} \quad (21)$$

δ_1 and δ_2 are the deflection values obtained for the un-cracked section and cracked section, respectively, and are determined from Eqs. 22 and 23 for beams subjected to four point bending conditions:

$$\delta_1 = \frac{Pa}{24E_c I_g}(3L^2 - 4a^2) \quad (22)$$

$$\delta_2 = \frac{Pa}{24E_c I_{cr}}(3L^2 - 4a^2) \quad (23)$$

In these expressions, P is the applied load at each point, L is the clear span and a is the distance between the support and the nearest loading point. I_g and I_{cr} are the second moment of area calculated on the basis of the un-cracked and cracked sections, respectively, determined using the expressions in Eqs. 24 and 25:

$$I_g = \frac{bh^3}{12} \quad (24)$$

$$I_{cr} = \frac{bd^3k^3}{3} + nA_s d^2(1-k)^2 \quad (25)$$

where $k = \sqrt{2\rho n + (\rho n)^2} - \rho n$

In Eq. 25, the term n refers to the modular ratio between the reinforcement and the concrete, given as the ratio of E to E_c.

In the current analysis, the deflection of the beam is calculated at the mid-span of the member at the service moment, which is 30% of the ultimate bending moment ($0.3M_u$), as well as at 67% of the ultimate bending moment ($0.67M_u$). Table 4 presents a comparison between the measured deflections from the numerical model (δ_{FE}) and the predicted values obtained using Eurocode 2 (δ_{EC2}), using the expressions given in Eqs. 19-25. The results presented in the table are for beams made from C40 concrete which are 300 mm in width and 428 mm in depth, and employ the elastic modulus for the stainless steel (E) in the calculations. In order to study the influence of the stainless steel constitutive relationship on the deflection of RC beams, various reinforcement ratios (ρ) are considered to develop different levels of stress in the reinforcement.

It is observed that the Eurocode 2 design deflections at $0.3M_u$ are in very good agreement with the corresponding numerical values (δ_{EC2}/δ_{FE}) with the maximum and average differences being around -38% and -2%, respectively. These same values at $0.67M_u$ are -28% and -15%, respectively. Figs. 24(a) and (b) demonstrate the influence that the reinforcement ratio has on the beam deflections at $0.3M_u$ and $0.67M_u$, respectively. It is clear that Eurocode 2 predictions are in very good agreement with the corresponding measured values from the FE model in almost all cases for beams which are at the service load, corresponding to a bending moment of $0.3M_u$. On the other hand, the code results in over-conservative predictions for beams with relatively higher reinforcement ratios, when the beam is subjected to $0.67M_u$. It is also observed that the deflections rise with an increase of reinforcement ratio up to specific point (i.e. at a reinforcement ratio of around 1%) after which remains more or less constant. This indicates that the deflection is more influenced by the reinforcement ratio for relatively low values of ρ, where the stress level in the reinforcement is relatively greater.

564 Table. 4: Results of the predicted deflection obtained from Eurocode 2 in comparison with the measured

565 values from the FE model.

Reinforcement ratio (ρ)	Grades	Bending moment		Deflections at $0.3M_u$			Deflections at $0.67M_u$		
		$0.3M_u$ (kNm)	$0.67M_u$ (kNm)	δ_{EC2} (mm)	δ_{FE} (mm)	δ_{EC2}/δ_{FE}	δ_{EC2} (mm)	δ_{FE} (mm)	δ_{EC2}/δ_{FE}
0.0019	1.4311	22.7	50.6	0.38	0.36	1.05	6.05	6.47	0.94
	1.4162	25.6	57.1	0.43	0.70	0.62	7.80	8.19	0.95
	1.4307	23.6	52.6	0.40	0.42	0.95	6.36	6.70	0.95
0.0039	1.4311	40.9	91.3	2.16	2.07	1.04	9.10	9.31	0.98
	1.4162	46.0	102.7	3.04	3.05	1.00	10.64	11.22	0.95
	1.4307	42.2	94.2	2.32	2.38	0.98	9.17	9.51	0.96
0.0078	1.4311	75.0	167.5	4.05	3.79	1.07	10.15	11.34	0.90
	1.4162	86.6	193.3	4.91	4.76	1.03	11.96	13.82	0.87
	1.4307	79.6	177.8	4.24	4.02	1.06	10.49	12.02	0.87
0.0117	1.4311	103.4	231.0	4.39	4.27	1.03	10.30	12.30	0.84
	1.4162	118.7	265.1	5.18	5.20	1.00	12.02	14.83	0.81
	1.4307	109.7	244.9	4.56	4.47	1.02	10.63	12.84	0.83
0.0156	1.4311	122.9	274.4	4.30	4.26	1.01	9.89	12.27	0.81
	1.4162	143.1	319.6	5.12	5.27	0.97	11.69	15.37	0.76
	1.4307	133.9	299.1	4.59	4.62	0.99	10.50	13.36	0.79
0.0216	1.4311	152.6	340.9	4.29	4.51	0.95	9.73	13.27	0.73
	1.4162	158.6	354.2	4.52	4.78	0.94	10.23	14.15	0.72
	1.4307	157.2	351.0	4.31	4.53	0.95	9.76	13.28	0.74

566

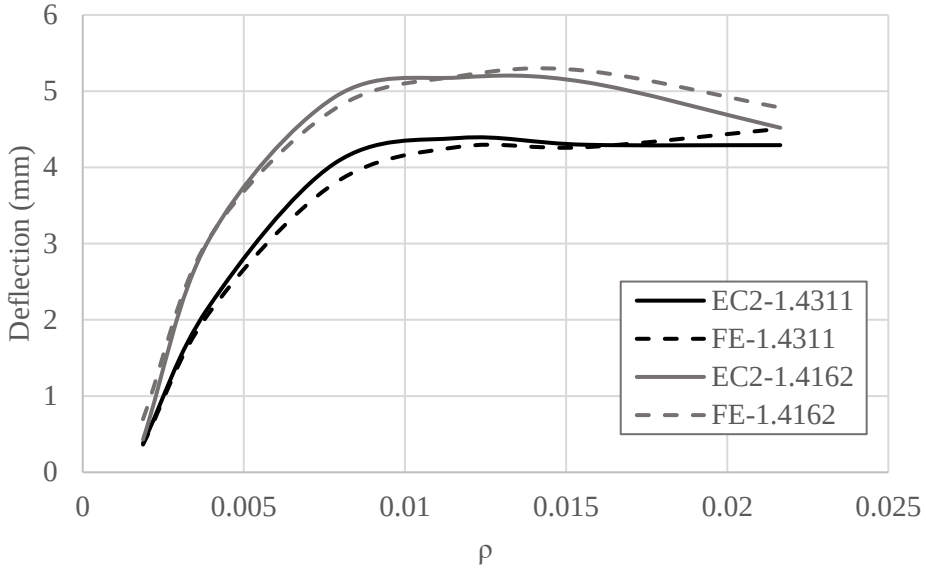

(a)

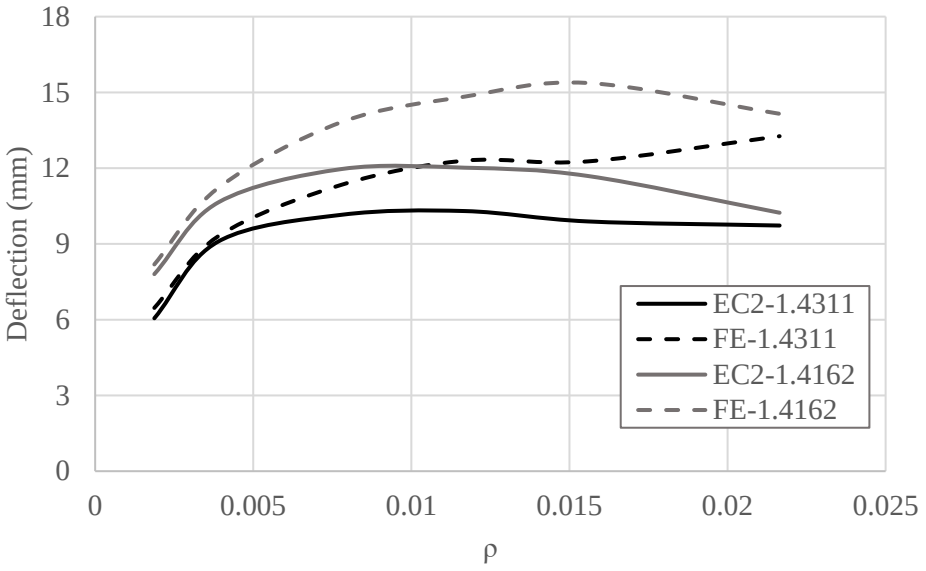

(b)

Fig. 24: Effect of reinforcement ratio on the deflection of a stainless steel reinforced concrete beam at (a) $0.3M_u$ and (b) $0.67M_u$.

As stated before, the current design approach in Eurocode 2 [6] calculates the deflection on the basis of the modulus of elasticity of the reinforcement. This assumption is acceptable in the case of carbon steel reinforcement, however it may result in an over-conservative prediction in the case of stainless steel

reinforcement owing to its nonlinear behaviour. In the design of structural stainless steel sections, it is recommended to use the secant modulus in deflection calculations rather than the elastic modulus [37]. In order to investigate this for reinforced concrete design, the predicted deflections calculated using secant modulus and also the tangent modulus of the stainless steel reinforcement are compared with their corresponding numerical values.

The secant modulus of elasticity (E_{sec}) for stainless steel is obtained from the modified Ramberg-Osgood material model presented earlier in Eqs. 1 and 2 according to:

$$E_{sec} = \frac{E}{1+0.002\frac{E}{\sigma}\left(\frac{\sigma}{\sigma_{0.2}}\right)^{n}} \quad \text{for} \quad \sigma \leq \sigma_{0.2} \tag{26}$$

$$E_{sec} = \frac{\sigma}{\varepsilon_{0.2} + \frac{\sigma - \sigma_{0.2}}{E_2} + \left(\varepsilon_u - \varepsilon_{0.2} - \frac{\sigma_u - \sigma_{0.2}}{E_2}\right)\left(\frac{\sigma - \sigma_{0.2}}{\sigma_u - \sigma_{0.2}}\right)^{m}} \quad \text{for} \quad \sigma_{0.2} < \sigma \leq \sigma_u \tag{27}$$

The tangent modulus of elasticity (E_{tan}) is the derivative of the secant modulus and is determined as follows:

$$E_{tan} = \frac{\sigma_{0.2}\, E}{\sigma_{0.2} + 0.002\, n\, E\left(\frac{\sigma}{\sigma_{0.2}}\right)^{n-1}} \quad \text{for} \quad \sigma < \sigma_{0.2} \tag{28}$$

$$E_{tan} = \frac{1}{\frac{1}{E_2} + \left(\varepsilon_u - \varepsilon_{0.2} - \frac{\sigma_u - \sigma_{0.2}}{E_2}\right)\left(\frac{m}{(\sigma_u - \sigma_{0.2})^{m}}\right)(\sigma - \sigma_{0.2})^{m-1}} \quad \text{for} \quad \sigma_{0.2} < \sigma \leq \sigma_u \tag{29}$$

The deflection of elastic beams (i.e. those not containing a plastic hinge) may be estimated by standard structural theory. In order to obtain the secant modulus and the tangent modulus of the reinforcement at $0.3M_u$ and $0.67M_u$, the stress in the reinforcement must first be determined. An elastic analysis of the section is conducted to obtain the depth of the neutral axis (y) and the stress in the reinforcement, according to the stress and strain distributions presented in Fig. 25.

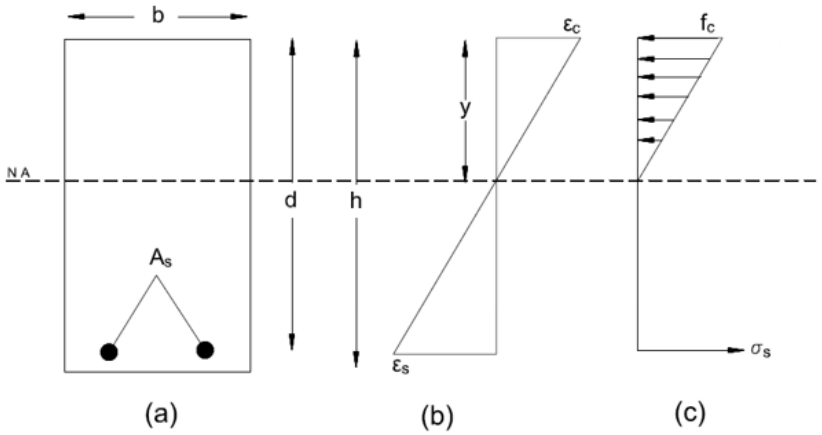

590

591 Fig. 25: Elastic analysis of a reinforced concrete beam including (a) the cross-section (b) the strain
592 distribution, (c) the stress distribution in the section.

593 The location of the neutral axis can be obtained from Eq. 30:

$$y = d\left(\sqrt{2\rho n + \rho^2 n^2} - \rho n\right) \tag{30}$$

594 where n is the modular ratio between the reinforcement and concrete:

$$n = \frac{E_{sec}}{E_c} \quad \text{for secant modulus}$$
$$n = \frac{E_{tan}}{E_c} \quad \text{for tangent modulus} \tag{31}$$

595 Once the neutral axis depth is located, the stress in the reinforcement is calculated from the stress
596 distribution in Fig. 25(c), as follows:

$$\sigma_s = \frac{M_a}{A_s(d - y/3)} \tag{32}$$

597 Since the secant and tangent moduli are functions of the stress in the reinforcement, an iterative
598 technique is required to obtain the solution of Eq. 32. A flow chart describing the solution procedure
599 for determining the secant modulus is given in Fig. 26. The same solution procedure can be followed
600 to determine the tangent modulus. Then, the deflections of the beam for load levels corresponding to
601 $0.3M_u$ and $0.67M_u$ are calculated using secant modulus and the tangent modulus.

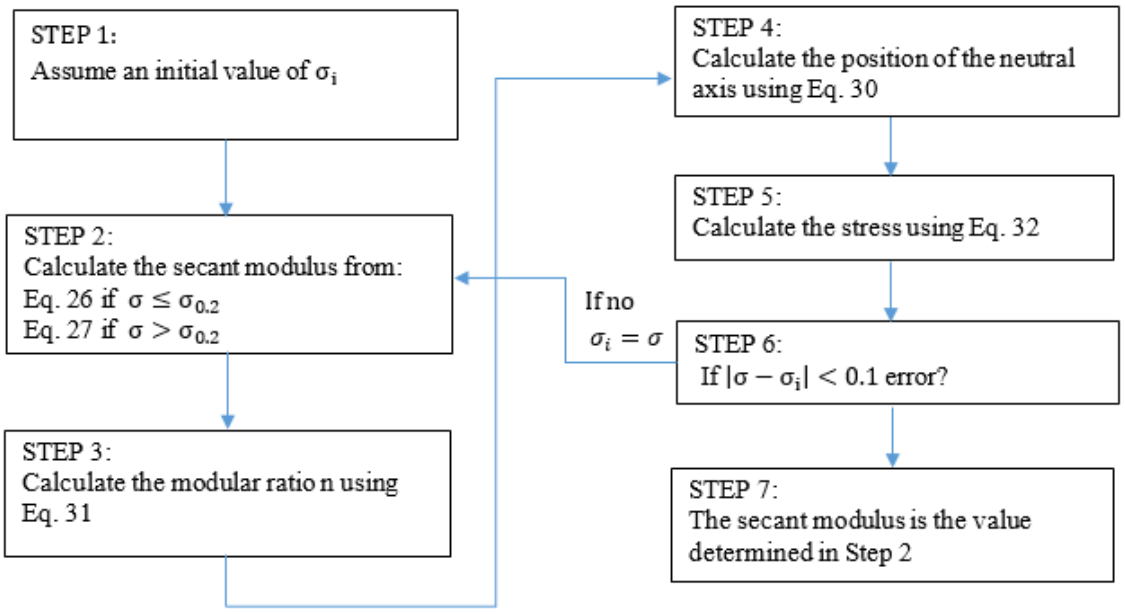

Fig. 26: Flow chart of the solution procedure.

The predicted deflections obtained using the elastic modulus (δ_{EC2}), secant modulus ($\delta_{EC2(Esec)}$) and tangent modulus ($\delta_{EC2(Etan)}$) for the stainless steel grades considered herein, are presented in Table 5 in comparison with the corresponding numerical values (δ_{FE}). The results show that implementing the secant modulus in the calculations of deflection provides quite accurate predictions at $0.3M_u$ with maximum and average $\delta_{EC2(Esec)}/\delta_{FE}$ values of -38% and 0%, respectively. However, these results are quite similar in terms of accuracy as the corresponding deflections obtained using the elastic modulus of stainless steel, as presented earlier, which gave maximum and average δ_{EC2}/δ_{FE} values of -38% and -2%, respectively. On the other hand, at $0.67M_u$, using the secant modulus in deflection calculations results in un-conservative predictions with maximum and average $\delta_{EC2(Esec)}/\delta_{FE}$ values of 55% and 18%, respectively. The corresponding values when the elastic modulus is used in the calculations are -28% and -15%, respectively, as previously presented.

Using the tangent modulus in deflection calculations at load levels corresponding to $0.3M_u$ results in maximum and average $\delta_{EC2(Etan)}/\delta_{FE}$ values of -38% and 6%, respectively, whilst at $0.67M_u$ the maximum and average $\delta_{EC2(Etan)}/\delta_{FE}$ values are 1130% and 205%, respectively. It is clear that the using the tangent

618 modulus to calculate the deflections results in a significant overestimation of the deflections compared
619 with the numerical model values, especially at higher load levels.

620 In summary, the results presented in this analysis show that there is only a minor improvement in the
621 deflection predictions by adopting the secant modulus rather than the elastic modulus in the
622 calculations, and in all cases at load levels corresponding to $0.3M_u$, conservative predictions are
623 achieved. The predictions obtained using the tangent modulus were significantly less accurate than
624 when the elastic modulus or the secant modulus is employed. Therefore, it is recommended to use the
625 elastic modulus in the calculation of deflections for stainless steel RC beams. It is noteworthy that the
626 predicted deflections for beams with a reinforcement ratio 0.187% at loads corresponding to $0.3M_u$ are
627 typically the same for each stainless steel grade considered herein. After a careful examination of these
628 cases, it was found that applied load is lower than the cracking moment and therefore the deflection is
629 calculated only on the basis of an un-cracked section. In this scenario, the second moment of area is
630 calculated based on the gross area of the section which is the same irrespective of the reinforcement
631 modulus of elasticity.

632 Table. 5: Deflection results obtained using the initial modulus, secant modulus and the tangent modulus

633 of stainless steel in comparison with the measured values from the FE model.

Reinforcement ratio	Grade	Bending moment (kNm)		Deflections at $0.3M_u$			Deflections at $0.67M_u$		
		0.3Mu	0.67Mu	δ_{EC2}/δ_{FE}	$\delta_{EC2(Esec)}/\delta_{FE}$	$\delta_{EC2(Etan)}/\delta_{FE}$	δ_{EC2}/δ_{FE}	$\delta_{EC2(Esec)}/\delta_{FE}$	$\delta_{EC2(Etan)}/\delta_{FE}$
0.00187	1.4311	22.7	50.6	1.05	1.05	1.05	0.94	1.36	12.30
	1.4162	25.6	57.1	0.62	0.62	0.62	0.95	1.35	2.89
	1.4307	23.6	52.6	0.95	0.95	0.95	0.95	1.46	4.02
0.00390	1.4311	40.9	91.3	1.04	1.09	1.29	0.98	1.48	5.91
	1.4162	46.0	102.7	1.00	1.01	1.05	0.95	1.26	2.45
	1.4307	42.2	94.2	0.98	1.01	1.11	0.96	1.55	3.60
0.00779	1.4311	75.0	167.5	1.07	1.12	1.29	0.90	1.41	3.60
	1.4162	86.6	193.3	1.03	1.04	1.08	0.87	1.09	1.94
	1.4307	79.6	177.8	1.06	1.08	1.19	0.87	1.33	2.79
0.01169	1.4311	103.4	231.0	1.03	1.06	1.19	0.84	1.35	2.94
	1.4162	118.7	265.1	1.00	1.00	1.03	0.81	0.96	1.52
	1.4307	109.7	244.9	1.02	1.04	1.12	0.83	1.15	2.17
0.01559	1.4311	122.9	274.4	1.01	1.03	1.11	0.81	1.14	2.16
	1.4162	143.1	319.6	0.97	0.98	0.99	0.76	0.85	1.21
	1.4307	133.9	299.1	0.99	1.01	1.06	0.79	1.01	1.72
0.02165	1.4311	152.6	340.9	0.95	0.97	1.02	0.73	0.94	1.57
	1.4162	158.6	354.2	0.94	0.95	0.95	0.72	0.76	0.90
	1.4307	157.2	351.0	0.95	0.96	0.99	0.74	0.85	1.23

634

635 # 5. Conclusions

636 This paper has presented a detailed investigation into the behaviour of stainless steel reinforced concrete
637 beams. A full and simplified version of a deformation-based design method for the analysis of these
638 elements has been proposed and examined in comparison with predictions of the current design rules
639 in Eurocode 2. A comprehensive parametric study was conducted to study the influence that various
640 geometric and material properties have on the capacity of the members. Moreover, the paper provides
641 guidance for selecting an appropriate reinforcement ratio in order to allow for an evaluation of the
642 strain hardening properties of the stainless steel reinforcement being included in the design. In the
643 final section of the paper, the serviceability limit state for stainless steel reinforced concrete beams has
644 been explored through a detailed analysis of the deflection behaviour. Overall, the results and analysis
645 presented in this paper have provided an excellent basis for engineers to specify stainless steel
646 reinforcement in reinforced concrete beams in an efficient and sustainable manner, with minimal
647 wastage of materials. Following this detailed study, the following key findings and recommendations
648 for international codes of practice are presented:

649 1. The proposed full and simplified analytical approach is shown to be an effective design tool
650 that exploits the distinctive characteristics of stainless steel reinforcement in an efficient and
651 reliable manner.
652 2. For the range of data examined here, the average and maximum full analytical-to-numerical
653 bending moment values are -14.9% and -22.3% whilst these same values obtained using the
654 Eurocode 2 design rules are -28.3% and -44.7%, respectively.
655 3. The predictions of the simplified proposed analytical model are in excellent agreement with
656 the predictions of the full analytical model with the average and maximum full-to-simplified
657 bending moment values are -2.8% and -17.2%, respectively
658 4. In general, it is shown that further exploitation of the strain hardening capacity in the rebar is
659 achieved when a relatively higher grade of concrete is employed.
660 5. It is also found that the b/h ratio of the beam has a relatively small influence on the
661 exploitation of strain hardening.

6. It is observed that the levels of stress in the rebar are relatively lower when a higher reinforcement ratio is employed.
7. It is recommended that the elastic modulus is employed in the calculation of deflections for stainless steel RC beams rather than the secant modulus or the tangent modulus.
8. Finally, although the results presented herein are very promising in terms of improving the efficiency of designing stainless steel reinforced concrete beams, it is important that the shear resistance is studied in future work, including how the revised flexural capacities determined herein are likely to affect the design shear resistance.

References

[1]. BS EN 10088-1:1995: Stainless steels. List of stainless steels(1995), British Standards Institute.

[2]. Smale, K. (2018) 'From the scene | Collapsed Italy bridge laid bare'. Available at: https://www.newcivilengineer.com/latest/from-the-scene-collapsed-italy-bridge-laid-bare-17-08-2018/ (Accessed: 18 September 2019).

[3]. Markeset, G., Rostam, S. and Klinghoffer, O. (2006) 'Guide for the use of stainless steel reinforcement in concrete structures', Norwegian Building Research Institute, Norway.

[4]. Kalina R. D., Mac Lean S., and Breen J. E. (2011) 'Comparative Study of Mechanical and Corrosion Resistance Properties of Bridge Post-Tensioning Strands', The Center for Transportation Research at The University of Texas. Austin.

[5]. Gedge, G. (2003) 'Rationale for using stainless steel reinforcement in the UK construction industry', Arup Materials Consulting, UK.

[6]. EN 1992-1-1. (2004) 'Eurocode 2: Design of concrete structures part 1-1: General rules and rules for buildings', European Committee for Standardization (CEN).

[7]. Colajanni, P., Recupero, A. and Spinella, N. (2016) 'Increasing the flexural capacity of RC beams using steel angles and pre-tensioned stainless steel ribbons', Structural Concrete, 17(5), pp.848-857.

687 [8]. Colajanni, P., Recupero, A. and Spinella, N., 2017. 'Increasing the shear capacity of reinforced
688 concrete beams using pretensioned stainless steel ribbons'. Structural Concrete, 18(3), pp.444-
689 453.
690 [9]. Hassanein, M. and Silvestre, N. (2013) 'Flexural behavior of lean duplex stainless steel girders
691 with slender unstiffened webs', Journal of Constructional Steel Research, 85, pp. 12-23.
692 [10]. Wang, Y., Yang, L., Gao, B., Shi, Y. and Yuan, H. (2014) 'Experimental study of lateral-
693 torsional buckling behavior of stainless steel welded I-section beams', International Journal of
694 Steel Structures, 14(2), pp. 411-420.
695 [11]. Gardner, L. and Theofanous, M. (2008) 'Discrete and continuous treatment of local buckling
696 in stainless steel elements', Journal of Constructional Steel Research, 64(11), pp. 1207-1216.
697 [12]. Huang, Y. and Young, B. (2014) 'Design of cold-formed lean duplex stainless steel members
698 in combined compression and bending', Journal of Structural Engineering, 141(5), pp.
699 04014138.
700 [13]. Ramberg, W. and Osgood, W.R. (1943) 'Description of stress-strain curves by three
701 parameters', Issue 902 of National Advisory Committee for Aeronautics Technical Note.
702 [14]. Mirambell, E. and Real, E. (2000) 'On the calculation of deflections in structural stainless
703 steel beams: an experimental and numerical investigation', Journal of Constructional Steel
704 Research, 54(1), pp. 109-133.
705 [15]. Rasmussen, K.J.R. (2003) 'Full-range stress–strain curves for stainless steel alloys', Journal of
706 Constructional Steel Research, 59(1), pp. 47-61.
707 [16]. Hasan, M.A., Akiyama, M., Kashiwagi, K., Kojima, K. and Peng, L., 2020. Flexural
708 behaviour of reinforced concrete beams repaired using a hybrid scheme with stainless steel
709 rebars and CFRP sheets. Construction and Building Materials, 265, p.120296.
710 [17]. Hasan, M.A., Yan, K., Lim, S., Akiyama, M. and Frangopol, D.M., 2020. LCC-based
711 identification of geographical locations suitable for using stainless steel rebars in reinforced
712 concrete girder bridges. Structure and Infrastructure Engineering, 16(9), pp.1201-1227.
713 [18]. Gardner L., Nethercot D.A. (2004) ‘Structural stainless steel design: a new approach’. Journal
714 of Structural Engineering, 82(21),pp. 21-30.

715 [19]. Ashraf, M., Gardner, L. and Nethercot, D.A. (2008) 'Structural stainless steel design:
716 resistance based on deformation capacity', Journal of Structural Engineering, 134(3), pp. 402-
717 411.
718 [20]. Gardner, L., Wang, F. and Liew, A. (2011) 'Influence of strain hardening on the behavior and
719 design of steel structures', International Journal of Structural Stability and Dynamics, 11(05),
720 pp. 855-875.
721 [21]. Lan, X., Chen, J., Chan, T. and Young, B. (2018) 'The continuous strength method for the
722 design of high strength steel tubular sections in compression', Engineering Structures, 162, pp.
723 177-187.
724 [22]. Gardner, L., Yun, X., Macorini, L. and Kucukler, M. (2017) 'Hot-rolled steel and steel-
725 concrete composite design incorporating strain hardening', Structures, 9, pp. 21-28.
726 [23]. Shamass, R. and Cashell, K.A., (2018) 'Analysis of Stainless Steel-Concrete Composite
727 Beams', Journal of Constructional Steel Research, 152, pp. 132-142.
728 [24]. Rabi, M., Cashell, K. and Shamass, R. (2019) 'Flexural analysis and design of stainless steel
729 reinforced concrete beams', Engineering Structures, 198, pp. 109432.
730 [25]. Rabi, M., Cashell, K.A. and Shamass, R. (2019) 'Analysis of concrete beams reinforced with
731 stainless steel', Proceedings of the fib Symposium 2019: Concrete-Innovations in Materials,
732 Design and Structures, pp. 690-697.
733 [26]. Abdella, K. (2006) 'Inversion of a full-range stress–strain relation for stainless steel alloys',
734 International Journal of Non-Linear Mechanics, 41(3), pp. 456-463.
735 [27]. Rabi, M., Cashell, K.A., Shamass, R. and Desnerck, P., 2020. Bond behaviour of
736 austenitic stainless steel reinforced concrete. Engineering Structures, 221, p.111027.
737 [28]. Dassault Systèmes. (2016) Abaqus user's Guide Manual [Computer program].
738 http://dixon:2080/texis/search/?query=concrete+materialandgroup=bkandCDB=v2016andsubm
739 it.x=0andsubmit.y=0.
740 [29]. Wang, T. and Hsu, T.T. (2001) 'Nonlinear finite element analysis of concrete structures using
741 new constitutive models', Computers and Structures, 79(32), pp. 2781-2791.

742 [30]. Alfano, G., De Cicco, Ph. D, Fiorenzo and Prota, A. (2011) 'Intermediate debonding failure of
743 RC beams retrofitted in flexure with FRP: Experimental results versus prediction of codes of
744 practice', Journal of Composites for Construction, 16(2), pp. 185-195.
745 [31]. Obaidat, Y.T., Heyden, S., Dahlblom, O., Abu-Farsakh, G. and Abdel-Jawad, Y. (2011)
746 'Retrofitting of reinforced concrete beams using composite laminates', Construction and
747 Building Materials, 25(2), pp. 591-597.
748 [32]. Alih, S. and Khelil, A. (2012) 'Behavior of inoxydable steel and their performance as
749 reinforcement bars in concrete beam: Experimental and nonlinear finite element analysis',
750 Construction and Building Materials, 37, pp. 481-492.
751 [33]. Dong, J., Wang, Q. and Guan, Z. (2013) 'Structural behaviour of RC beams with external
752 flexural and flexural–shear strengthening by FRP sheets', Composites Part B: Engineering,
753 44(1), pp. 604-612.
754 [34]. Li, Q., Guo, W., Liu, C., Kuang, Y. and Geng, H., (2020). Experimental and Theoretical
755 Studies on Flexural Performance of Stainless Steel Reinforced Concrete Beams. Advances in
756 Civil Engineering, 2020.
757 [35]. Medina, E., Medina, J.M., Cobo, A. and Bastidas, D.M. (2015) 'Evaluation of mechanical and
758 structural behavior of austenitic and duplex stainless steel reinforcements', Construction and
759 Building Materials, 78, pp. 1-7.
760 [36]. Gardner, L., Bu, Y., Francis, P., Baddoo, N.R., Cashell, K.A. and McCann, F. (2016)
761 'Elevated temperature material properties of stainless steel reinforcing bar', Construction and
762 Building Materials, 114, pp. 977-997.
763 [37]. SCI. (2017) 'Design Manual for Structural Stainless Steel', fourth edition, SCI Publication No.
764 P413. The Steel Construction Institute.

765